

Document downloaded from:

<http://hdl.handle.net/10251/181379>

This paper must be cited as:

Rueda-García, L.; Bonet Senach, J.L.; Miguel Sosa, P.; Fernández Prada, M.Á. (2021). Analysis of the shear strength mechanism of slender precast concrete beams with cast-in-place slab and web reinforcement. *Engineering Structures*. 246:1-18.
<https://doi.org/10.1016/j.engstruct.2021.113043>



The final publication is available at

<https://doi.org/10.1016/j.engstruct.2021.113043>

Copyright Elsevier

Additional Information

1 Analysis of the shear strength mechanism of slender precast 2 concrete beams with cast-in-place slab and web reinforcement

3 Lisbel Rueda García, lisruega@cam.upv.es

4 José Luis Bonet Senach, jlbonet@cst.upv.es

5 Pedro Fco. Miguel Sosa, pmiguel@cst.upv.es

6 Miguel Ángel Fernández Prada, mafernan@cst.upv.es

7 *Universitat Politècnica de València, Camí de Vera s/n, 46022, Valencia, Spain*

8 **Abstract**

9 Precast concrete beams with cast-in-place slabs on top, namely concrete composite beams
10 are frequently used for building concrete bridge decks. In designs, the contribution of cast-
11 in-place slabs to shear strength tends to be omitted. However, given the vast number of
12 existent bridges with this deck typology, significant cost savings could be made when
13 assessing these structures if the slab's shear strength is considered. This paper analyses
14 how cast-in-place slab influences the shear behaviour of concrete composite beams with
15 web reinforcement. For this purpose, an experimental programme of 18 concrete
16 specimens with web reinforcement and rectangular cross-sections was run, in which the
17 following parameters varied: cross-sectional depth; existence of an interface between
18 concretes; compressive strengths of the concrete of beams and slabs; differential shrinkage
19 between concretes. It was observed that: the slab contributed to resist shear; the existence
20 of an interface between concretes led to a crack appearing along it that caused the
21 transmitted shear to be divided into two load paths: one through the precast beam and
22 another one through the slab; the slab's concrete strength was that which mainly influenced
23 the element's shear strength; differential shrinkage did not reduce shear strength. Based on
24 experimental observations, a mechanical model is proposed in this paper to assess the

1 composite elements' shear strength, which considers the yielding of both stirrups and the
2 slab's longitudinal reinforcement to be a failure criterion, which well predicted the
3 experimental results. The shear formulations of Eurocode 2, the Level III Approximation of
4 Model Code 2010 and the (b) Formula of ACI 318-19 offered a similar result to the herein
5 proposed method when using the entire composite element effective depth and the
6 weighted average of the concrete strengths of both the beam and slab estimated from the
7 area ratio. Codes significantly underestimated specimens' interface shear.

8 **Keywords:** precast construction, reinforced concrete, composite beam, shear strength,
9 shear failure, mechanical model, design, assessment.

10 **Highlights**

11 Shear in monolithic and composite beams with stirrups was experimentally tested

12 Slab contributed to increase composite specimens' shear strength

13 The interface between concretes modified the shear strength mechanism

14 A mechanical model of composite specimens' shear strength is proposed

15 The proposed model well fits this test programme's experimental results

1. Introduction

The report conducted by the Technical Committee 4.3 “Road bridges” of PIARC in 2016 [1] revealed that at least 50% of the participating countries’ bridges are made of reinforced or prestressed concrete; particularly in Europe, this percentage is more than 80% on average. To construct these concrete bridges, a very common deck typology has often been used since the mid-20th century, which consists in precast concrete beams with a cast-in-place slab on top, commonly known as concrete composite beams (Fig. 1). Given the considerable number of existent decks with this typology, it is especially important to study their structural behaviour.

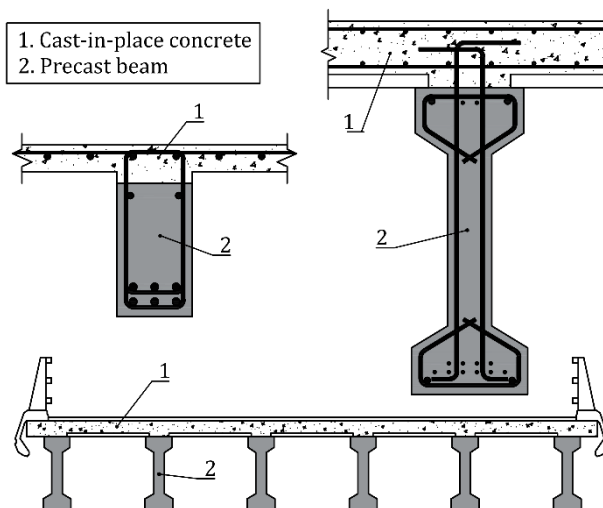


Fig. 1. Examples of the cross-sections of precast beams with cast-in-place slabs frequently used in concrete composite beams decks.

The interface between concretes in concrete composite beams is a weakness plane whose premature failure may limit both the element’s vertical and horizontal shear strengths [2]. The research work carried out on composite beams has traditionally focused on analysing the interface shear [3–8], mainly to analyse the effect of interface roughness, the shear span-depth ratio, concretes’ properties and the interface’s shear reinforcement. However, a few experimental studies in the existent literature have analysed the vertical shear behaviour of reinforced concrete composite beams [9].

1 In vertical shear designs of reinforced concrete composite beams, the contribution of the
2 cast-in-place slab to shear strength is usually neglected because it remains on the safety
3 side. However, the slab's contribution could be significant to assess the shear strength of
4 existing bridge decks made of precast concrete beams and cast-in-place slabs as increased
5 shear strength due to cast-in-place slab's contribution can imply substantial maintenance
6 cost savings in these infrastructures [9], which derive from reducing the need for their
7 reinforcement, or even their replacement. Hence the importance of studying whether the
8 cast-in-place concrete slab resists shear in composite beams, in which way and how much
9 it can resist.

10 In general, current design codes' shear formulations do not describe the shear strength
11 prediction when, as is common in composite beams, the concretes' compressive strengths
12 of the precast beam and the cast-in-place slab differ. Only ACI 318-19 [10] in Section 22.5.4
13 specifies how this shear strength can be calculated: using the concrete compressive strength
14 of the element (precast beam or cast-in-place slab) that results in the most critical shear
15 strength value or the properties of the individual elements. However today, relevant
16 experimental and theoretical evidence is not sufficient to support the validity of the design
17 code for composite beams [9,11]. EC2 [12] in Section 10.9.3(8) allows the design of concrete
18 elements with a topping of at least 40 mm thick as composite elements if the shear at the
19 interface is verified. Other codes like MC-10 [13] do not refer to this type of structural
20 elements.

21 In the scientific literature, several publications [14–23] are about the experimental analysis
22 of full-scale concrete composite beams with web reinforcement. Most have focused on
23 analysing the verification of these elements' shear capacity according to design code'
24 formulations. However, these studies have not analysed either the contribution of the cast-
25 in-place concrete slab to the composite beam's shear strength or how the existence of a joint
26 between concretes of different ages can affect shear behaviour.

1 According to Halicka [2], there is little number of research works regarding the influence of
2 the interface cracking on the composite unit's shear resistance. She performed an
3 experimental study on the influence of interface quality on concrete composite beams' shear
4 strength, in which she proposes a classification of failure mechanisms of concrete composite
5 beams. According to this classification, interface shear failure will take place when the shear
6 force that initiates interface cracking is less than the shear force that results in diagonal
7 cracking appearing, which will limit the element's ultimate vertical shear strength. On the
8 contrary, if diagonal cracking occurs first, two situations can be observed: the shear that
9 produces interface cracking is lower than the element's ultimate shear strength, in which
10 case the trajectory of diagonal cracks will be modified along the interface before penetrating
11 the upper chord; the shear that produces interface cracking is higher than the element's
12 ultimate shear strength, in which case the composite beam will behave like a monolithic
13 beam. The second failure mode will be the structurally desired behaviour as the interface is
14 not a weakness plane for shear strength. However, the first failure mode can be common,
15 especially in elements with either significant differential shrinkage between the concrete of
16 the beam and that of the slab, or changes in the section width (T-shaped beams) [24,25],
17 and deserves to be studied.

18 Kim *et al.* [11] ran an experimental programme about the shear strength of rectangular
19 composite beams with shear reinforcements. Their study focused mainly on analysing the
20 existence of different class concretes (high-strength and low-strength concretes) at the
21 beam and slab. They obtained results on the relation between the shear strength of
22 composite beams and the compressive strengths of the beam and slab's concretes and the
23 beam and the slab's depth. This provided information about the extent to which each
24 composite beam part contributes to shear strength. However, both transverse
25 reinforcement and interface roughness in these experimental tests meant that the interface
26 shear strength was high. Thus the failure mode was barely affected generally by the
27 existence of an interface, and the behaviour of these specimens was similar to the

1 monolithic one according to the Halicka classification [2]. Their study, therefore, did not
2 analyse how the existence of an interface would influence shear strength.

3 In a previous study carried out by the authors [26], the shear strength of 21 monolithic and
4 concrete composite beams, with rectangular and T-shaped cross-sections and with no web
5 reinforcement, was analysed. The main findings of the rectangular composite specimens
6 were that: 1) the existence of a slab on top of the beam improved its shear strength; 2) the
7 interface between concretes could modify the critical shear crack shape, consequently, the
8 shear strength mechanism; 3) the use of high-strength concrete in the precast beam slightly
9 increased its shear strength; 4) the differential shrinkage between the concretes of the
10 precast beam and the cast-in-place slab did not significantly influence composite specimens'
11 vertical shear capacity; 5) the design codes generally provided better estimations of actual
12 strengths when the entire composite beam depth and individual elements' shear strengths
13 were used, and gave results on the interface shear that were very much on the safety side.

14 Following these previous studies, the present research work studies how the cast-in-place
15 slab influences the shear behaviour of concrete composite beams with web reinforcement.
16 The specific aim is to analyse the shear strength mechanism of rectangular reinforced
17 concrete composite beams with web reinforcement, particularly in those composite beams
18 in which the existence of an interface between concretes substantially modifies the shear
19 strength mechanism, unlike what happens when beams display monolithic behaviour. To
20 this end, 18 monolithic and composite rectangular specimens, with equal and different
21 cross-sectional depths, compressive strengths of the beam and slab's concretes, and
22 different concrete ages, were experimentally tested. The obtained results, as well as the
23 different introduced variables, are analysed. Based on the experimental results, a
24 mechanical model for assessing the shear strength of the composite beams in the
25 experimental programme is proposed, which can be used as a reference for the future
26 development of a method to assess composite beams' shear strength. Both the proposed

1 model and the formulations for calculating the shear strength of current design codes are
2 verified with the experimental programme results.

3 The main contributions of this research work are, on the one hand, to increase the number
4 of available experimental tests in this field and, on the other hand, to provide a better
5 understanding of the shear transfer mechanism in composite beams whose elements have
6 different quality concretes. This will allow researchers to propose mechanical-based design
7 and assessment formulations for such elements to improve their safety and prolong their
8 service life.

9 **2. Test programme**

10 **2.1. Test parameters**

11 In order to analyse the contribution of cast-in-place concrete slabs to the shear strength of
12 a rectangular composite beam with web reinforcement, and how the existence of an
13 interface between concretes can affect its shear behaviour, the following four variables
14 were studied:

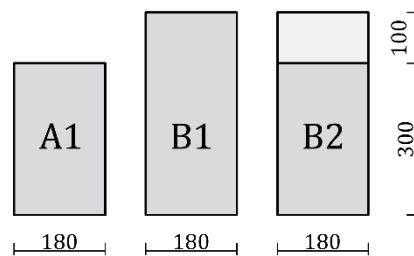
15 (a) Cross-sectional depth. Firstly, a reference section type A, which represented the
16 precast beam used in composite elements. Secondly, a section type B with an
17 increased depth compared to section A (see [Fig. 2](#))

18 (b) The existence of an interface between concretes. Beams were fabricated with one
19 concrete (monolithic beams A1 and B1 in [Fig. 2](#)) or two concretes (composite
20 beams, compound of a beam with a cast-in-place slab on top: B2 in [Fig. 2](#))

21 (c) Strengths of the beam and slab's concretes. Two types of concretes were used to
22 fabricate specimens: normal-strength concrete (NSC) with a design compressive
23 strength of 30 MPa, which represented a concrete traditionally used in cast-in-place
24 construction; a concrete with higher compressive strength (HCS), with a design
25 compressive strength of 50 MPa, which represented a concrete often used in precast

1 concrete plants. In the composite specimens, the influence of the beam's concrete
2 compressive strength was studied using NSC or HCS on the beam, while the slab's
3 concrete compressive strength was fixed to a conventional concrete (NSC)

4 (d) Differential shrinkage between concretes. Most composite specimens were
5 fabricated with concretes of similar ages (24-hour difference) for a faster
6 construction process and to reduce the differential shrinkage between the beam and
7 slab's concretes. However, in order to analyse if the use of different ages concretes,
8 common in precast construction, had a significant influence on the shear strength of
9 the composite specimens in this experimental programme, the slab's concrete was
10 poured later into two composite beams once the beam's concrete shrinkage
11 stabilised.



12
13 *Fig. 2. Cross-section types (dimensions: mm).*

14 The following parameters were fixed to avoid their influence on the study:

- 15 • Interface roughness ("smooth" or "as-cast"). The beam's concrete underwent no
16 further treatment after vibration, so the interface between beam and slab's
17 concretes was "smooth" or "as cast", as described in current design codes [12,13]
- 18 • Longitudinal reinforcement ratio ($\rho_l = 4.0\%$). Longitudinal reinforcement was
19 designed to avoid the bending failure of all beams
- 20 • Shear reinforcement ratio ($\rho_w = 0.22\%$). The web reinforcement design met the
21 most restrictive minimum spacing requirements between stirrups of all the codes
22 used to design these beams [10,12,13]

- 1 • The shear span-effective depth ratio ($a/d = 4.0$). a/d was chosen based on the
2 observations of Kani's valley [27] to foster shear failure
- 3 • Relative concrete cover ($c/h = 0.16$). The concrete cover met the design codes'
4 specified minimums

5 Both interface roughness and the shear reinforcement ratio were chosen based on the
6 observations made by a previous research work carried out by the authors [28], in which
7 beams with the same characteristics as those in this experimental programme showed that
8 the smooth interface, together with vertical shear reinforcement, were enough to obtain the
9 beam's diagonal cracking prior to interface cracking. This proved the interface treatment's
10 effectiveness in neither failing in interface shear nor showing monolithic behaviour, even
11 though the code calculations predicted interface shear failure. Smooth interface roughness
12 is also the roughness that is often left in precast concrete plants.

13 This experimental programme fabricated 18 reinforced concrete beams with web
14 reinforcement, divided into three series: NW, HW and DW. The beam and slab's concrete
15 types employed in the series, the number of days that elapsed between the beam's concrete
16 pouring and the slab's concrete pouring in the composite specimens, and the number of
17 specimens per series, are shown in Table 1. In the composite specimens of series NW and
18 DW, the compressive strengths of the beam and slab's concretes were similar (NSC in both),
19 while different concrete compressive strengths were used in series HW (HCS on the beam
20 and NSC on the slab).

21 *Table 1. Series of the experimental programme.*

Series	Type of beam's concrete	Type of slab's concrete	Days between beam and slab's concrete pouring	Number of specimens per cross-sectional type		
				A1	B1	B2
NW	NSC	NSC	1	3	3	4
HW	HCS	NSC	1	2	2	2
DW	NSC	NSC	134	0	0	2

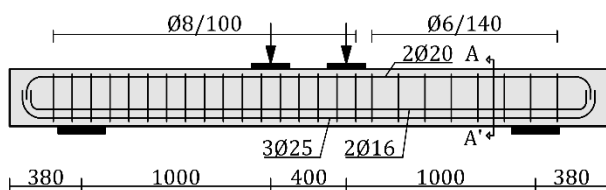
22 Specimen designation was carried out using $xWPyzk(j)$, where: " xW " denoted the name of
23 the series (NW for the specimens with NSC on the beam, HW for the specimens with HCS on

1 the beam and DW for the specimens fabricated with different aged concretes); “*P_y*” was the
 2 batch of concrete pouring (from P1 to P7 as the fabrication process was conducted 7 times);
 3 “*z*” denoted the cross-sectional shape (A or B in Fig. 2); “*k*” was the number of concretes
 4 that formed the specimen (1 for monolithic beams, 2 for composite beams); “*j*” (“*a*” or “*b*”)
 5 was used when more than one specimen with the same previously described characteristics
 6 was fabricated.

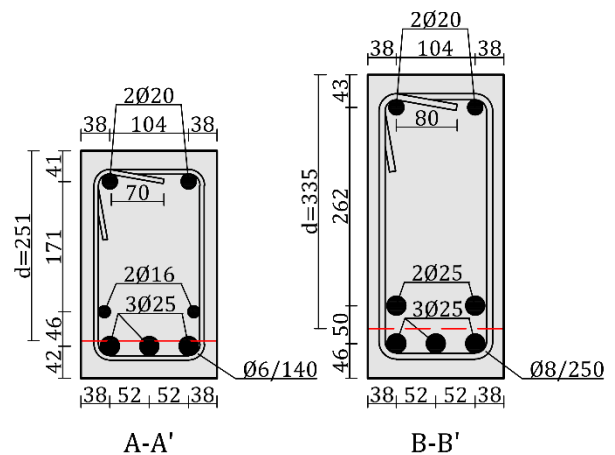
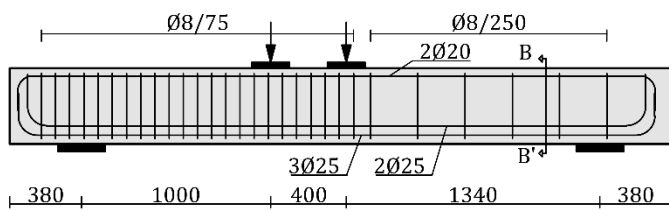
7 2.2. Test specimens

8 Fig. 3 shows specimens’ dimensions and reinforcement. The total length of the beams with
 9 section B was 3.50 m, with a distance of 2.74 m between supports. Two-point non-centred
 10 vertical loading was applied, with a 0.40 m distance between loads, which formed two
 11 spans: a 1.34-metre principal span, in which failure was expected, and resulted in fixed
 12 parameter $a/d = 4.0$, and a 1.00-metre span, reinforced to avoid its shear failure. The beams
 13 with section type A were designed with a 3.16 m length (2.40 m between supports) to obtain
 14 fixed parameter $a/d = 4.0$, with 1.00-metre principal and reinforced spans.

Section type A



Section type B



16 Fig. 3. Dimensions and reinforcement of beams type A and B (dimensions in mm).

17 In the composite beams (sections B2), two concrete layers were used. The first layer, 0.30
 18 m high, represented the precast beam. The second layer, 0.10 m high and cast on top of the
 19 previous one, represented the cast-in-place concrete slab.

1 **2.3. Fabrication of specimens**

2 Beams were fabricated in seven batches (P1 to P7 in Table 2), which allowed a comparison
3 to be made between the beams of the same batch without influencing the concrete strength
4 variable. The beam fabrication process was carried out in two phases. The first phase
5 consisted in beam's concrete pouring (concrete of the monolithic specimens and the precast
6 beam's concrete in the composite specimens). In all the composite beams, at the principal
7 span, where failure was expected, no surface treatment was performed after concrete
8 pouring. So the surface was "smooth" or "as-cast", according to current code definitions
9 [10,12,13]. The concrete surface of the reinforced span was raked before concrete hardened
10 to increase the interface shear strength. Dents of approximately 6 mm deep (from peak to
11 valley) and a maximum spacing of 40 mm between peaks were made. A "very rough"
12 interface was created in this way as defined in the codes. Good workability conditions for
13 the concrete casting were sought. Table 2 shows the measured slump of the first phase
14 concretes because their consistency can influence surface roughness. The slump test was
15 done in accordance with UNE-EN 12350-2 [29].

1 *Table 2. Summary of the test results.*

Series	Fabrication batch	Specimen	$f_{c,28,b}$ (MPa)	$f_{c,28,s}$ (MPa)	f_{cb} (MPa)	f_{cs} (MPa)	$E_{c,b}$ (MPa)	$E_{c,s}$ (MPa)	$f_{ct,b}$ (MPa)	$f_{ct,s}$ (MPa)	Slump beam (cm)	V_{exp} (kN)	$\tau_{h,exp}$ (MPa)	
NW	P1	NWP1B2	32	32	33	32	33535	37689	2.61	2.27	6.0	206	3.79	
		P2	NWP2A1	37	-	37	-	33421	-	2.99	-	17.5	158	-
	P2	NWP2B1	-	-	37	-	33421	-	2.99	-	-	181	-	
		NWP2B2	-	34	39	34	31961	30428	2.58	2.50	-	186	3.43	
		P3	NWP3A1	32	-	33	-	32927	-	2.58	-	22.5	128	-
	P3	NWP3B1	-	-	31	-	32927	-	2.58	-	-	174	-	
		NWP3B2	-	38	32	37	32927	33854	2.58	3.21	-	169	3.12	
		P4	NWP4A1	39	-	39	-	28652	-	2.79	-	18.0	153	-
	P4	NWP4B1	-	-	39	-	28300	-	2.86	-	-	168	-	
		NWP4B2	-	33	40	33	26413	28715	3.04	2.48	-	191	3.53	
		HW	P5	HWP5A1	43	-	43	-	24633	-	2.58	-	20.0	144
	P5		HWP5B1	-	-	42	-	24662	-	2.40	-	-	207	-
HWP5B2			-	22	43	22	24633	20098	2.58	2.01	-	172	3.17	
P6	HWP6A1	52	-	52	-	28651	-	2.86	-	24.0	(*)	-		
	HWP6B1	-	-	52	-	28395	-	2.86	-	-	199	-		
	HWP6B2	-	36	52	36	28395	29458	2.86	3.01	-	186	3.44		
DW	P7	DWP7B2a	24	36	29	37	24939	31243	2.44	2.82	15.0	167	3.09	
		DWP7B2b	-	-	29	37	24939	31243	2.44	2.82	-	179	3.30	

Notation:

Suffix "b" refers to beam's concrete.

Suffix "s" refers to slab's concrete.

(*) V_{exp} could not be measured because of failure detected during the test process.

2 The second fabrication phase consisted in the slab's concrete being poured on the
3 composite specimens and subsequent concrete curing for the next 7 days. In beams NW and
4 HW, this phase was carried out 24 h after the first phase to, thus, reduce differential
5 shrinkage between concretes as much as possible. In beams DW, this second phase took
6 place 134 days after the first phase when the beam's concrete shrinkage measurements
7 indicated that it was stabilised.

8 In all the fabricated specimens, the entire length of beam was laid on the floor when the
9 slab's concrete was being poured. Hence in this experimental programme, both the beam
10 and slab were loaded at the same time.

11 **2.4. Material properties**

12 The mechanical characterisation of the used concretes was carried out according to UNE-
13 EN 12390 [30–32]. The results obtained were the average of two concrete cylinders (300

1 mm high, 150 mm diameter), tested at the age of 28 days and every day a specimen was
2 tested. Beams were tested approximately 28 days after the fabrication process. The average
3 values of the compressive strengths of the beam and slab's concretes measured at the age
4 of 28 days ($f_{c,28}$) are offered in Table 2, which also shows the average values of the
5 compressive strengths of the beam and slab's concretes ($f_{c,b}$ and $f_{c,s}$ respectively), the
6 moduli of elasticity E_c and the tensile concrete strengths f_{ct} (calculated as the 90% of the
7 tensile splitting strength of concrete, according to [33]) measured on the day when each
8 specimen was tested. The average coefficients of variation of these measurements were 2,
9 3 and 7% for the compressive strength, the modulus of elasticity and the tensile strength of
10 concretes, respectively.

11 For concrete dosage, the water-cement ratio, the amount of Portland cement and the
12 maximum aggregate size were 0.52, 325 kg/m³ and 10 mm for NSC, and 0.44, 500 kg/m³
13 and 10 mm for HCS, both respectively.

14 The mechanical properties of reinforcing steel were obtained according to UNE-EN ISO
15 6892 [34]. Steel type was C class according to classification of EC2-04 [12]. Two pieces of
16 reinforcing steel of each nominal diameter were tested to obtain the average values of the
17 steel mechanical properties shown in Table 3. It should be noted that the stirrups used in
18 all the specimens (except the specimens of series NWP1) were made of the same steel so
19 that the comparison of beams' shear strength provided by stirrups did not depend on steel
20 properties.

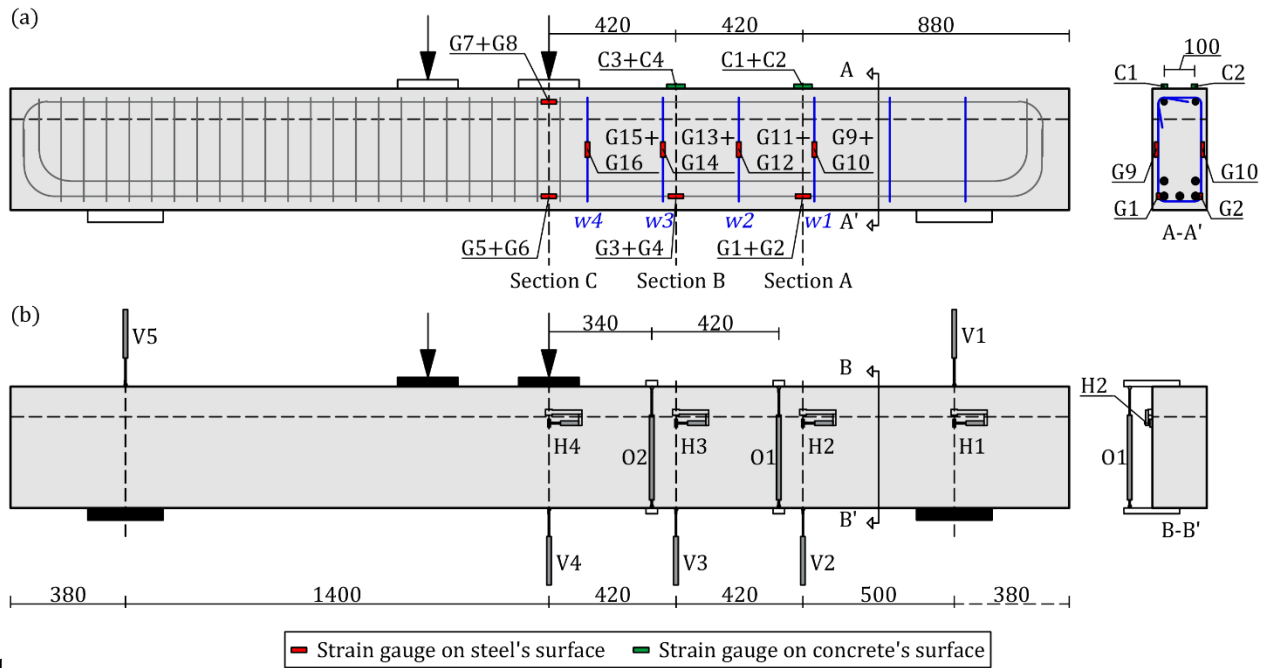
1 *Table 3. Average values of the reinforcing steel properties.*

	Series	\varnothing (mm)	f_y (MPa)	E_s (GPa)	ε_y (‰)	f_u (MPa)	ε_u (%)
Stirrups	NWP1	8	534	189	2.8	662	10.1
	Rest of series	6	534	227	2.4	666	11.0
		8	538	203	2.7	658	12.0
Longitudinal reinforcement	NWP1	20	534	206	2.6	639	10.5
		25	556	197	2.8	670	9.7
	NWP2, NWP3, NWP4, DWP7	16	561	240	2.3	675	31.9
		20	585	192	3.0	673	41.0
		25	557	199	2.8	666	48.3
	HWP5	16	545	230	2.4	655	31.7
		20	541	194	2.8	654	26.7
		25	548	235	2.3	658	21.6
	HWP6	16	531	231	2.3	641	33.2
		20	560	190	2.9	675	22.0
		25	574	237	2.4	687	19.2

2 2.5. Instrumentation

3 Three 1000 kN load cells were used to measure the hydraulic jack force and the reactions
4 at the two bearing points.

5 Strain gauges (120 Ω resistance and 2 mm measuring length) were placed on some steel
6 reinforcing bars surface to measure strains. As shown in Fig. 4a, three pairs of strain gauges
7 (G1 to G6) were placed at three different cross-sections upon tension longitudinal
8 reinforcement (Sections A, B and C). Below the central point load, a pair of strain gauges
9 was placed on compression longitudinal reinforcement (G7 and G8). Pairs of strain gauges
10 were glued in the middle of the two legs of four stirrups (stirrups w1 to w4 in Fig. 4a) of the
11 principal span (five stirrups for beams type A) (gauges G9 to G16 in Fig. 4a).



1
2 *Fig. 4. Instrumentation of a type B2 beam for the shear test: (a) strain gauges; (b) LVDTs (dimensions in mm).*

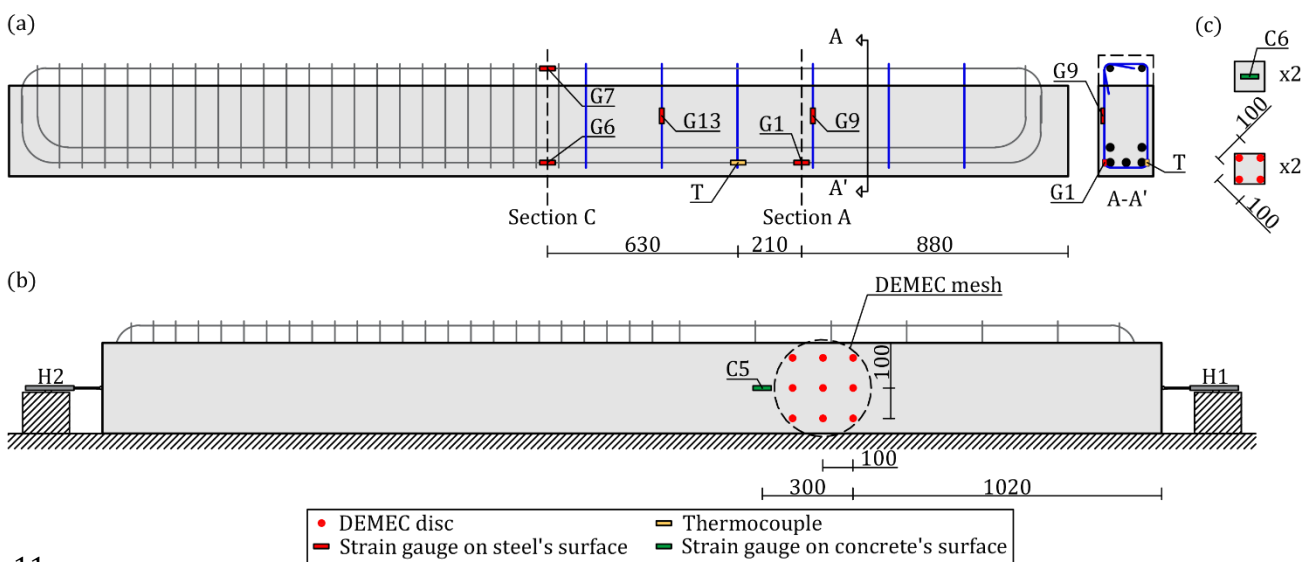
3 On the concrete surface of beams type B, two strain gauges (120 Ω resistance and 60 mm
4 measuring length), separated from one another by 100 mm, were placed at Sections A and
5 B in Fig. 4a (gauges C1 to C4 in Fig. 4a).

6 While testing, linear variable displacement transformers (LVDTs) were used. They took
7 continuous measurements of displacements on concrete surfaces. As shown in Fig. 4b, four
8 LVDTs were placed horizontally to measure the slip at the interface in the composite beams
9 (H1 to H4). Five LVDTs (V1 to V5) measured vertical displacements at the supports and at
10 Sections A, B and C. Two more vertical LVDTs, O1 and O2, were connected to the top and
11 bottom of beams to detect the beginning of cracking at either the interface or the web.

12 Two digital cameras took pictures during testing at a rate of 0.5 Hz and a high-speed camera
13 recorded brittle failures.

14 In the two beams of series DW, concrete's shrinkage was monitored for 4 months starting
15 from day 2 after beam's concrete pouring. As shown in Fig. 5, five strain gauges glued to the
16 steel surface (G1, G6, G7, G9 and G13 in Fig. 5a), and one strain gauge glued to the concrete
17 lateral surface (C5 in Fig. 5b), were connected to a data acquisition system to take

1 continuous strain measurements during the shrinkage test. A 3x3 discs mesh was placed on
 2 the concrete lateral surface (Fig. 5b) to measure deformations twice weekly by a
 3 demountable mechanical strain gauge (DEMEC). Two horizontal LVDTs were placed at the
 4 beam's ends to take continuous beam length shortening measurements (H1 and H2 in Fig.
 5 5b). A thermocouple glued to the steel surface (T in Fig. 5a) measured internal temperature,
 6 while a digital thermo-hygrometer recorded the ambient temperature and humidity
 7 throughout the shrinkage test. Additionally, two control concrete cubes (100x100x100
 8 mm), like that represented in Fig. 5c, were fabricated with the beam's concrete of series DW.
 9 Free shrinkage was measured by placing two strain gauges on the surface of each cube, and
 10 two 2x2 discs meshes for the DEMEC measurements. The shrinkage test lasted 112 days.



11
 12 *Fig. 5. Instrumentation of a DW beam for the shrinkage test: (a) internal instrumentation; (b) external*
 13 *instrumentation; (c) concrete cube instrumentation (dimensions in mm).*

14 2.6. Test setup and procedure

15 A steel-loading frame was used to perform shear tests (Fig. 6a). The vertical load was
 16 applied by means of a 1200 kN hydraulic jack with displacement control (0.02 mm/s). The
 17 hydraulic actuator load was divided into two point loads by means of a steel frame with a
 18 joint to keep the load vertical (Fig. 6b). Load was transmitted to beams through two steel
 19 plates (200x200x30 mm). Beams were laid on two bearing points. As shown in Fig. 6c, they

1 were made of a steel plate (250 mm width), a steel balls bed to eliminate the horizontal
2 reaction and a joint to allow rotations on the plane of the steel-loading frame.

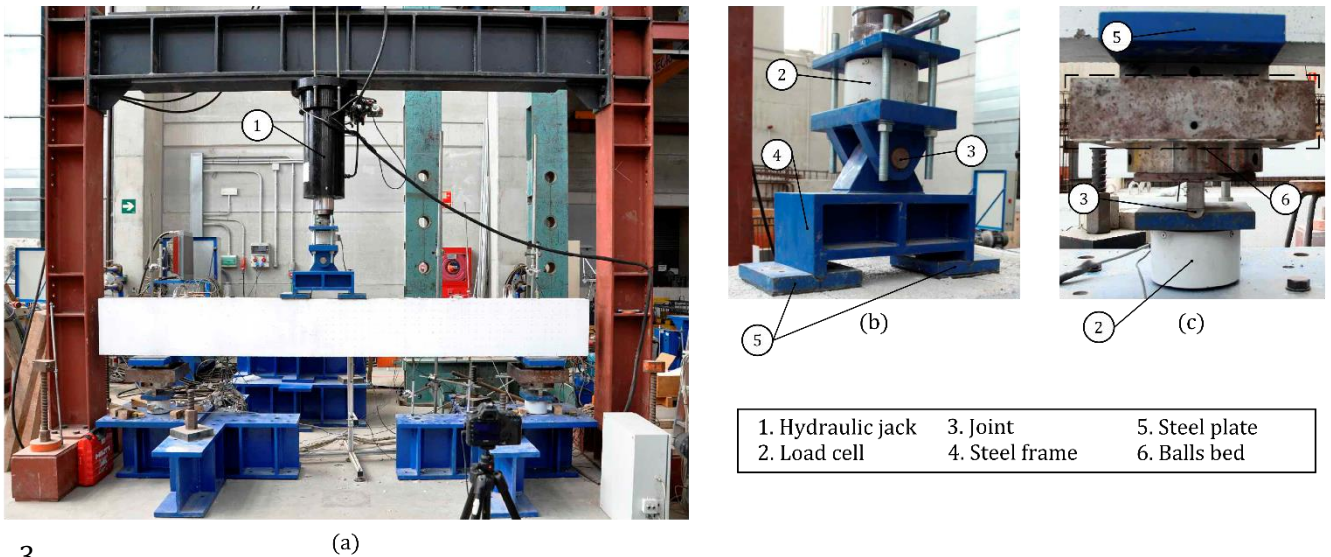


Fig. 6. Shear test experimental setup: (a) global view; (b) loading system; (c) bearing points system.

3. Test results and Discussion

3.1. Shear-deflection relation

Fig. 7 shows the relation between the shear force at the principal span V and the deflection below the point load closest to that span (LVDT V4 in Fig. 4b) of all test specimens, except beam HWP6A1, due to failure during the test process. The maximum shear force reached during tests (V_{exp}) and the shear force correspondent to the first diagonal crack appearing ($V_{diag,crack}$) are highlighted on curves. The $V_{diag,crack}$ value was obtained from the instrumentation results as the shear force for which significant strains were recorded for the first time in one of the instrumented stirrups (Fig. 4a) or large displacements in LVDTs O1 or O2 (see Fig. 4b), and by verifying the results with the test pictures.

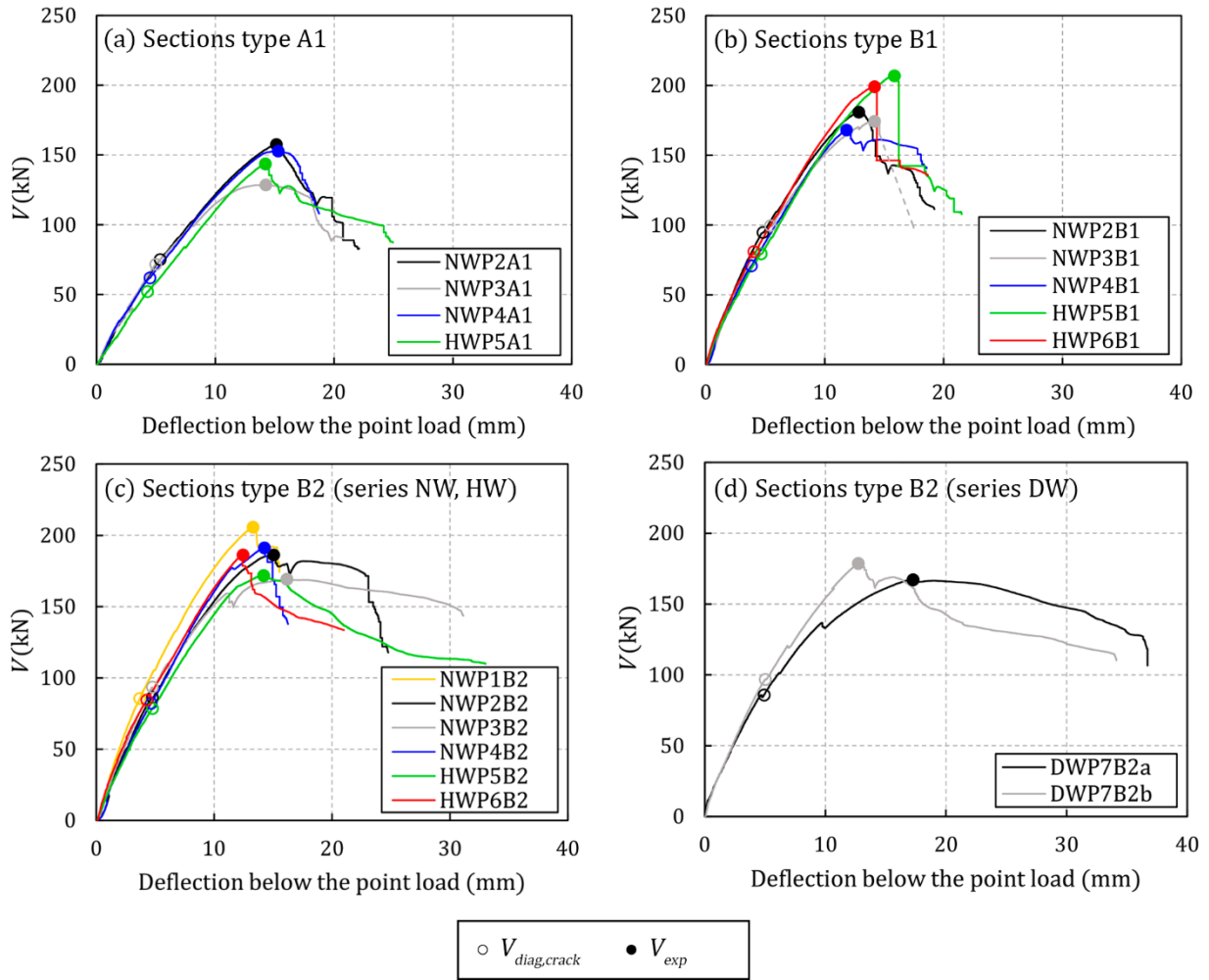


Fig. 7. Shear-deflection relation of test specimens: (a) sections type A1; (b) sections type B1; (c) sections type B2 from series NW and HW; (d) sections type B2 from series DW (specimen HWP6A1 not included: test process failure).

3.2. Shear strength

The vertical shear strength value of the test specimens (V_{exp}) is shown in Table 2. This table also indicates the interface shear stress concurrent with V_{exp} ($\tau_{h,exp}$), calculated as $V_{exp}/(0.9bd)$, as indicated in EC2 [12] and used by previous authors [11], based on equilibrium conditions, for the composite specimens of this experimental programme.

3.3. Crack pattern observations

The principal span crack patterns of all the beams in this experimental programme are shown in Fig. 8. The existent cracks when maximum shear V_{exp} was reached are represented, as are the cracks that occasionally appeared immediately after V_{exp} with a sudden load drop (e.g., see specimen HWP6B1 in Fig. 7), and the cracks observed at the end of tests.

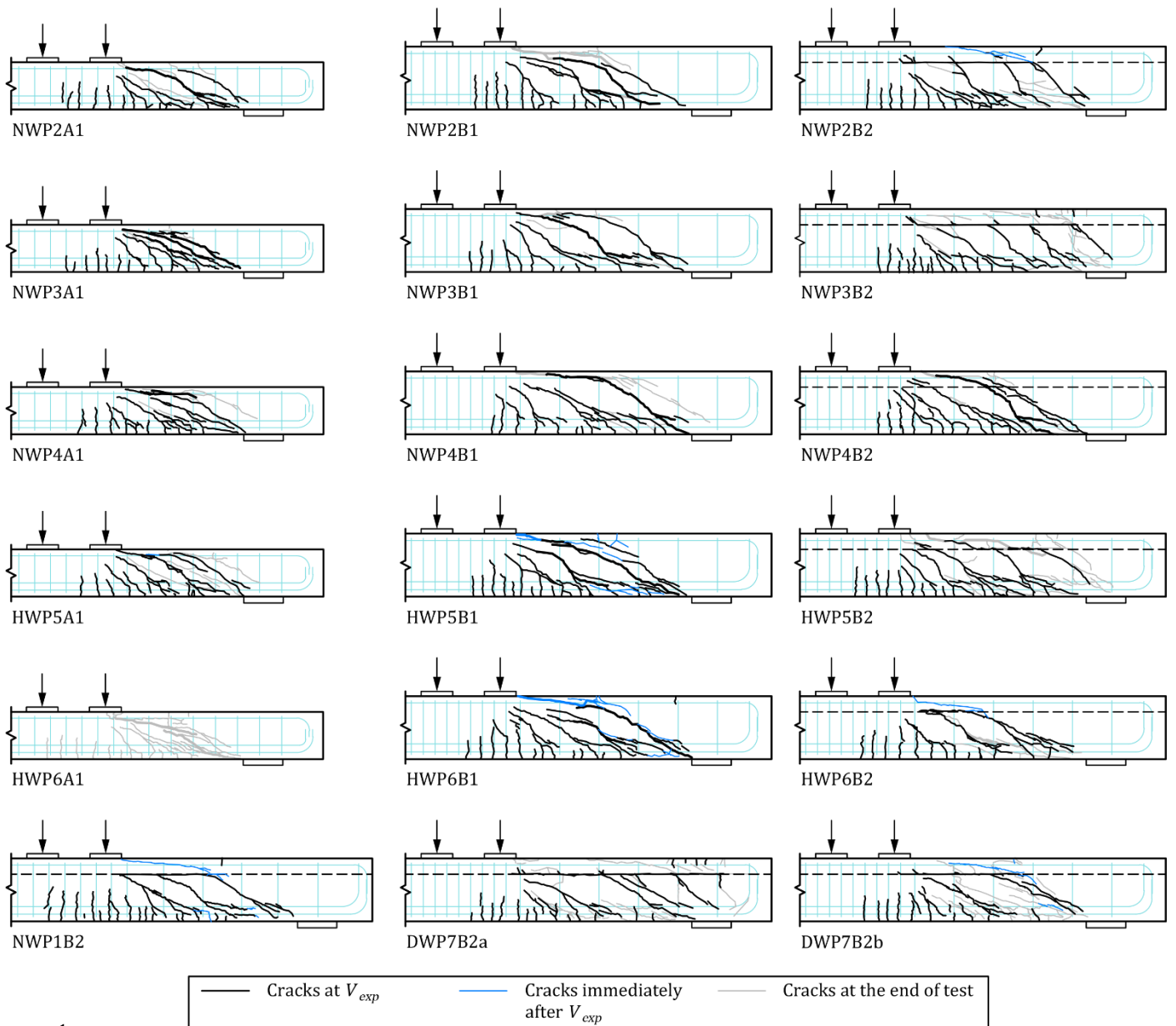


Fig. 8. Crack patterns of the test specimens in different test stages.

1
2
3 In the first load stages, all the specimens showed similar cracking propagation. The first
4 observed cracks were bending cracks. These cracks appeared in the region of almost pure
5 bending and extended vertically up to the beam's neutral axis (cracks observed in the area
6 below the point load in Fig. 8), exactly as early research observed [35]. With increasing load,
7 more bending cracks appeared along beams' principal span. The cracks in the zone below
8 the load remained vertical, while the shear span cracks curved towards the point load after
9 surpassing the tension longitudinal reinforcement level.

1 At a shear force between 36 and 57% of maximum shear, a diagonal crack opened during
2 tests (see $V_{diag,crack}$ at Fig. 7). This opening was detected in the measurements of one of the
3 vertical LVDTs (O1 or O2 in Fig. 4b). Consequently, the strain gauges located on the stirrups
4 showed that the stirrup crossed by this crack underwent increased strain at that instant. As
5 load increased, new diagonal cracks appeared on the principal span and an increase in the
6 strain of the correspondent stirrup crossed by them took place.

7 When the diagonal cracks of the principal span exceeded the neutral axis depth, they
8 became flatter on a second branch. After this load stage, major differences in beams' crack
9 patterns were observed according to whether they were monolithic or composite.

10 *3.3.1. Rectangular monolithic beams*

11 In the rectangular monolithic beams (sections type A1 and B1), a variation in the inclination
12 of diagonal cracks was observed on this second branch when they penetrated the
13 compression chord (see Fig. 8). These diagonal cracks continued propagating through the
14 compression chord in the point load direction and through the tension chord in the
15 direction of the support as longitudinal cracks at the tension longitudinal reinforcement
16 level until maximum shear force V_{exp} was reached.

17 After V_{exp} , a progressive load drop occurred during which the critical shear crack
18 propagated towards the load plate (see NWP2A1 in Fig. 8). In some cases, the formation of
19 a longitudinal crack at the compression longitudinal reinforcement level or splitting of the
20 concrete cover along the compression longitudinal reinforcement was even observed (see
21 NWP2B1 and NWP4A1 in Fig. 8). Diagonal cracks progressed further towards the support
22 by means of cracks at the tension longitudinal reinforcement level.

23 *3.3.2. Rectangular composite beams*

24 In most of the tested beams with section type B2, while the inclination of the first branch of
25 diagonal cracks was similar to that of the monolithic beams, the second branch of cracks
26 took a horizontal direction, which was coincident with the interface between concretes. As

1 seen in Fig. 8, the second branches of the diagonal cracks spread until they connect to one
2 another along the shear span. Specimens NWP1B2, NWP2B2, NWP3B2, HWP6B2, DWP7B2a
3 and DWP7B2b displayed this behaviour. Vertical cracks at the top of the slab were observed
4 above the point at which the diagonal cracks closest to the support reached the interface
5 (e.g., see NWP3B2 in Fig. 8). The rest of the slab remained practically intact when beams
6 reached V_{exp} . Immediately after V_{exp} , some specimens showed a small load drop in relation
7 to a diagonal crack forming on the slab from the initial part of the interface crack closest to
8 the support in the point load direction (see the shear-deflection relation of specimens
9 NWP1B2, NWP2B2, HWP6B2 and DWP7B2b in Fig. 7 and their respective cracking patterns
10 in Fig. 8). Other specimens displayed very ductile behaviour, with a very progressive load
11 decrease, and without the formation of such a diagonal crack on the slab (see specimens
12 NWP3B2 and DWP7B2a in Fig. 7 and their cracking patterns in Fig. 8).

13 In the other tested composite specimens, the influence of the interface between concretes
14 on the trajectory of the diagonal cracks was less noticeable. Particularly in specimen
15 HWP5B2, the drift of the diagonal cracks along the interface was limited and the connexion
16 between the diagonal cracks at the interface did not take place at V_{exp} (see Fig. 8). After V_{exp} ,
17 some cracks on the slab appeared in specimen HWP5B2 during a gradual load decrease (see
18 Fig. 7 and Fig. 8). Specimen NWP4B2 showed a similar crack pattern to that of the
19 monolithic beams at both V_{exp} and the end of test. The critical shear crack did not change
20 direction when it crossed the interface between concretes.

21 The horizontal splitting of the concrete cover along the tension longitudinal reinforcement
22 was generally observed in all specimens.

23 **3.4. Instrumentation results**

24 Table 4 shows the main results obtained at V_{exp} from the strain gauges placed on the test
25 specimens (see Fig. 4a). The stirrup stress at mid-length is shown for the instrumented
26 stirrups of the principal span as σ_{s,w_i} where i is the number of stirrup (stirrups w1 to w4 in

1 Fig. 4a), calculated as the average of the strains measured by the two strain gauges located
 2 at each stirrup multiplied by the material's modulus of elasticity. The result was limited to
 3 the steel yield strength. Note that in the specimens with section type A1, with more stirrups
 4 on the principal span, the result for the stirrup w5 is also shown, which corresponds to the
 5 stirrup closest to the load plate. The average strains measured by the two pairs of strain
 6 gauges located on the concrete's surface in Sections A and B of Fig. 4a are also shown
 7 respectively as $\varepsilon_{c,SA}$ and $\varepsilon_{c,SB}$. Finally, the average of the strains measured by the two strain
 8 gauges located at the tension longitudinal reinforcement below the point load (gauges G5
 9 and G6 in Section C in Fig. 4a) is also shown in Table 4 as $\varepsilon_{s,l}$.

10 Table 4. Main results obtained from the instrumentation measurements at V_{exp} (specimen HWP6A1 not
 11 included: test process failure) (positive sign for compression).

Specimen	$\sigma_{s,w1}^{(1)}$ (MPa)	$\sigma_{s,w2}^{(1)}$ (MPa)	$\sigma_{s,w3}^{(1)}$ (MPa)	$\sigma_{s,w4}^{(1)}$ (MPa)	$\sigma_{s,w5}^{(1)}$ (MPa)	$\varepsilon_{c,SA}$ (‰)	$\varepsilon_{c,SB}$ (‰)	$\varepsilon_{s,l}$ (‰)
NWP1B2	-534	-534	-534	(2)	-	-	-	-2.39
NWP2A1	-534	-534	-534	-534	-532	-	-	-2.23
NWP2B1	-538	-538	-538	-511	-	-0.03	0.75	-1.85
NWP2B2	-502	-517	-451	-227	-	-4.06	1.40	-2.34
NWP3A1	-534	-534	-534	-534	-276	-	-	-1.83
NWP3B1	-538	-538	-538	-367	-	0.04	0.68	-1.89
NWP3B2	-538	-538	-538	-99	-	-0.15	1.63	-2.19
NWP4A1	(3)	-534	-534	-534	-354	-	-	-1.62
NWP4B1	-538	-538	-474	-168	-	0.36	1.43	-2.12
NWP4B2	-538	-538	-538	-359	-	-0.10	0.96	-2.21
HWP5A1	-534	-534	-534	-534	-365	-	-	-2.15
HWP5B1	-538	-538	-538	-538	-	-0.10	0.86	-2.53
HWP5B2	-538	-538	-538	-422	-	0.20	1.78	-2.03
HWP6B1	-538	-538	-538	-297	-	0.00	1.62	-2.14
HWP6B2	-538	-538	-538	-402	-	0.20	1.53	-2.11
DWP7B2a	-538	-532	-538	-54	-	0.16	1.11	-2.19
DWP7B2b	-538	-538	-538	-112	-	-0.18	1.10	-2.15

(1) Stresses calculated values with the strains measured by the strain gauges and the constitutive laws of the steel tested in laboratory.

(2) Non-instrumented stirrup in this test.

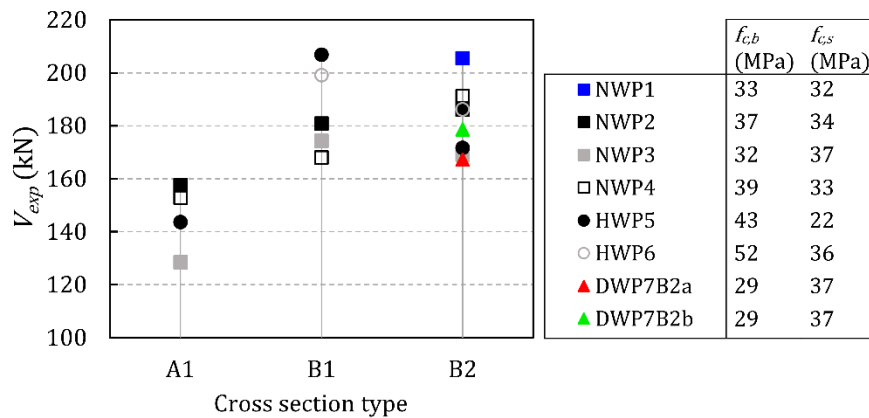
(3) The two strain gauges located on the stirrup failed.

12 Regarding the strain of the tension longitudinal reinforcement below the point load, it
 13 should be noted that in all the tests $\varepsilon_{s,l}$ was lower than the strain correspondent to the steel
 14 yield strength of the longitudinal reinforcement (approx. 2.8‰), which shows that
 15 specimens were far from the bending failure at V_{exp} .

1 On the other hand, on the DW series beams, it was observed that the value of the
 2 measurements taken by the instrumentation that controlled the beam's concrete shrinkage
 3 began to become asymptotic approximately 70 days after the shrinkage test started, which
 4 indicated that shrinkage had stabilised. The value of this asymptote for the free shrinkage
 5 measured by the gauges of the concrete control cubes (Fig. 5c) was an average strain of
 6 0.7‰. In the concrete strain gauges located at beams (C5 in Fig. 5b), the asymptote was
 7 reached at an average strain of 0.2‰, and at an average strain of 0.1‰ in the internal steel
 8 gauges (Fig. 5a). The internal temperature of beams and ambient temperature were, on
 9 average, 26°C, and the average ambient humidity was 64%.

10 3.5. Effect of test parameters on shear strength

11 Fig. 9 shows the shear strengths of the test specimens, including a summary table of the
 12 compressive strengths of the concretes used in both the beam and slab to facilitate finding
 13 differences due to the various introduced test parameters: the cross-sectional depth, the
 14 existence of an interface between concretes, the strength of the beam and slab's concretes
 15 and the differential shrinkage between concretes.



16
 17 Fig. 9. Experimental shear strength of test specimens and summary of compressive concrete strengths
 18 (specimen HWP6A1 not included: test process failure).

19 3.5.1. Cross-sectional depth

20 Regarding cross-sectional depth, the specimens with sections type A and B were compared
 21 to analyse the slab's contribution to shear strength. On average, the beams with sections

1 type B1 and B2 had 26% and 24% higher shear strengths, respectively, than the A1 beams
2 from the same fabrication batch. So it could be deduced that the cast-in-place slab
3 contributed to resist shear.

4 When only analysing the NW series with concretes of similar compressive strengths in both
5 the beam and slab, the depth enlargement in beams B1 and B2 increased shear strength in
6 relation to the A1 beams at a similar percentage (20% and 25% on average, respectively).
7 However, the depth increase of section B in relation to section A was 33%. The lesser
8 increase in the shear strength of beams type B1 in relation to depth increase could only be
9 explained by the size effect because the other parameters were identical. Therefore, as the
10 increase in shear strength of the B2 beams was similar to that of the B1 beams, it was
11 deduced that this lesser increase in the B2 beams' shear strength could also be due to the
12 size effect, and not to an interface existing between concretes.

13 Furthermore, the relation between beam height increase and shear strength increase of NW
14 specimens can be explained with coefficient k of equation 6.2 of EC2 [12], which accounts
15 for size effect. The relation between depth increase and shear strength increase was, on
16 average, 1.108 for the B1 specimens and 1.064 for the B2 specimens, what came close to the
17 relation between the k coefficients for A beams and B beams, which is 1.067.

18 In the beams with different compressive strength concretes at both the beam and slab (HW
19 series), it was not appropriate to draw conclusions because of, on the one hand, the
20 insufficient results obtained in the absence of the V_{exp} value of specimen HWP6A1 and, on
21 the other hand, the apparent dispersion shown by the series HWP5 specimens as specimen
22 HWP5A1 and specimen HWP5B1 acquired a lower and a higher shear strength than
23 expected, respectively, in view of the compressive strengths of their concretes.

24 *3.5.2. Existence of an interface between concretes*

25 The existence of an interface between concretes affected specimens' crack pattern, as
26 indicated in Section 3.3, causing in some cases cracks to develop along the interface. The

1 degree of cracking at the interface was a phenomenon that showed some dispersion, what
2 could be seen comparing the two composite specimens of series DW, which were
3 manufactured under equal conditions but presented somewhat different cracking (see Fig.
4 8). This finding proved the dispersion that concrete elements subjected to tangential
5 stresses (interface shear stresses in this case) display. However, certain variables that could
6 influence the degree of interface cracking of the specimens in this experimental programme
7 were found to exist. Regarding the specimens with reduced differential shrinkage between
8 concretes (series NW and HW), greater or lesser interface cracking could have been related
9 to the beam's concrete workability during casting (see the slump measurements in Table 2)
10 and concrete's setting time (which depended on the water-cement ratio, being the setting
11 faster in the concretes with a lower water-cement ratio). Thus we observed in the concretes
12 with a higher degree of workability and a higher water-cement ratio that the interface with
13 the "as-cast" roughness was smoother, which facilitated interface cracking during tests
14 *versus* the concretes with a lower degree of workability and a lower water-cement ratio,
15 whose interface was rougher. In the DW series beams, the previous variables could affect
16 interface cracking, but mainly the shrinkage stresses generated at the interface when there
17 is a difference in the shrinkage of the beam and slab's concretes [36] could be the cause of
18 the extended interface cracking in both test specimens.

19 When comparing the shear strengths of the specimens from the same fabrication batch with
20 section types B1 and B2 to analyse the influence of an existing interface, two behaviours
21 were distinguished: that of series NW and that of series HW. In the NW series specimens,
22 and regardless of the interface cracking type of specimens B2 (extended interface cracking
23 or cracking like a monolithic beam), the maximum shear was similar in beam B1 and beam
24 B2 from the same fabrication batch (see Fig. 9). Only in the NWP4 series did a major
25 difference appear between the specimens with sections B1 and B2. However, this difference
26 was attributed to the fact that the strength of specimen NWP4B1 was lower than expected.
27 It was deduced for the composite specimens in this experimental programme that for equal

1 concrete compressive strengths in both the beam and slab, the existence of an interface did
2 not significantly influence the specimen's shear strength compared to the same specimen
3 made with one concrete. Regarding the HW series specimens with different concrete
4 compressive strengths in both the beam and slab, the specimens with section type B2
5 showed lower shear strength than the B1 specimens (Fig. 9). In both HWP5 and HWP6, the
6 crack pattern of the beams type B2 at V_{exp} was scarcely affected by an interface existing
7 between concretes (see Fig. 8). Consequently, it was deduced that the lower shear strength
8 of the B2 specimens was due mainly to the existence of a lower compressive strength
9 concrete at the slab.

10 *3.5.3. Strengths of the beam and slab's concretes*

11 When comparing series NW to series HW, the higher concrete strength of the HW series in
12 the specimens with section type B1 provided higher shear strength, which was around 16%
13 higher (see specimens B1 in Fig. 9). In the composite beams, no appreciable differences
14 were observed in the V_{exp} of the series HW and NW beams, what could be due to the fact that
15 specimens' shear strength depended mainly on the compressive strength of the slab's
16 concrete which, in all the specimens of both series NW and HW, had a similar compressive
17 strength (normal-strength concrete, as shown in Table 1). Only specimen NWP1B2 had a
18 much higher V_{exp} than the average value recorded for the other composite specimens,
19 despite showing greater interface cracking than other specimens (see Fig. 8) and a lower
20 compressive strength of the slab's concrete than the other specimens did (see Fig. 9). Once
21 again, this demonstrated the scattering that can be found in shear.

22 *3.5.4. Differential shrinkage between concretes*

23 The shear strengths of the series NW specimens were compared to those of the series DW
24 specimens. The major differential shrinkage that took place between the beam and slab
25 concretes had no significant influence on the shear strength of the composite specimens as

1 similar shear strengths to those of the specimens with reduced differential shrinkage were
2 obtained (see Fig. 9).

3 **4. Shear strength mechanism**

4 **4.1. Failure mode description**

5 Until the time the first diagonal crack appeared, all the monolithic and composite specimens
6 showed the same shear strength mechanism as that observed in the reinforced concrete
7 beams with the same characteristics as those of this programme, and without web
8 reinforcement [26], as previously described by several authors [37,38]. Until the first
9 diagonal crack formed, shear was resisted by the combined action of the following shear
10 transfer actions: cantilever action, dowel action, aggregate interlock, residual tensile
11 strength of concrete, and the arching action or inclination of the compression strut above
12 cracks.

13 Whereas diagonal crack (critical shear crack) development entailed a maximum shear
14 strength of the element in the beams with no transverse reinforcement, the existence of
15 transverse reinforcement allowed it to absorb the tension forces that were generated in
16 concrete, and to vertically confine the compression chord and limit crack width to, thus,
17 contribute to increase the shear strength of the beam's web. This allowed specimens to
18 achieve higher shear strengths. Thus as new diagonal cracks developed from existing
19 bending cracks, beams' stirrups were activated; that is, their strain significantly increased
20 when they were crossed by a diagonal crack, as indicated in Section 3.3.

21 In monolithic specimens and in those composite specimens with quasimonolithic behaviour
22 (NWP4B2 and HWP5B2), in which the existence of the interface did not significantly modify
23 the crack pattern, it was observed that, as load increased, damage concentrated on one of
24 the diagonal cracks, the critical shear crack (see Fig. 8). As load increased, crack opening
25 also increased and, thus, the aggregate interlock, cantilever action and the residual tensile

1 strength of concrete decreased, and the strength of other mechanisms increased, such as
2 transverse reinforcement action, the dowel action of longitudinal reinforcement or arching
3 action, until a maximum shear strength was reached (V_{exp}). Afterwards, failure occurred
4 with sudden crack extension towards the loading point due to a shear failure of the
5 compression chord.

6 However, in the remaining composite beams of this experimental programme (NWP1B2,
7 NWP2B2, NWP3B2, HWP6B2, DWP7B2a, DWP7B2b), diagonal cracks developed along the
8 interface and clearly separated the lower beam, or precast beam, from the top slab, which
9 delayed the penetration of diagonal cracks into the compression chord. Fig. 8 shows that at
10 V_{exp} the diagonal cracks of the indicated specimens did not penetrate the top slab, so it
11 remained intact. Thus in the precast beam, with many diagonal cracks, the main shear
12 strength mechanisms were web reinforcement, the dowel action of longitudinal
13 reinforcement and the aggregate interlock. Interface cracking development cancelled
14 mechanisms like cantilever action between cracks. The slab could behave as a compressed
15 element that transmitted shear like an element with no shear reinforcements. The
16 connection between both elements (precast beam and slab) took place through the
17 activation of other shear strength mechanisms: the dowel action of transverse
18 reinforcement when it was crossed by the interface crack or the aggregate interlock in the
19 interface crack. After V_{exp} , sudden failure in some specimens occurred due to the formation
20 of a diagonal crack that crossed the slab (see specimens NWP1B2, NWP2B2, HWP6B2 and
21 DWP7B2b in Fig. 8), which denoted the shear failure of the compression chord, while others
22 displayed more ductile failure due to the slab's bending failure (see specimens NWP3B2 and
23 DWP7B2a in Fig. 8).

24 **4.2. Proposed shear strength mechanical model for the composite beams**

25 Based on the failure mode observations, a mechanical model for assessing the shear
26 strengths of the composite specimens of this experimental programme is proposed. The

1 model for calculating the shear strength of the composite specimens with interface cracking
2 is first described. After that, the experimental evidence that support the proposed model
3 are presented. Finally, the application of the proposed model to the composite specimens of
4 the experimental programme when the extension of the interface crack is unknown is
5 described.

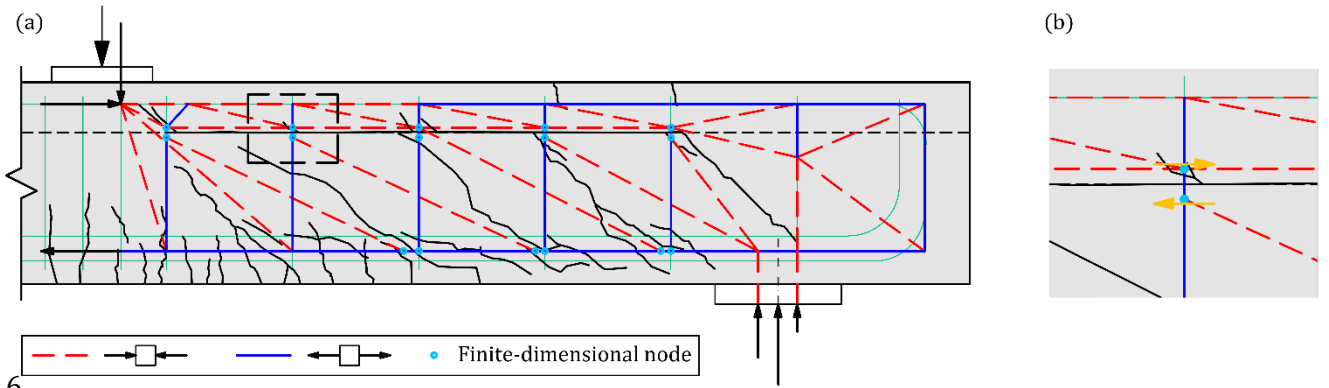
6 It should be noted that the proposed model was developed for its use in the shear strength
7 assessment of this experimental programme's composite specimens, providing a better
8 understanding of the shear strength mechanism developed by this type of elements that
9 could be used as a reference for the future development of a method to assess composite
10 beams' shear strength. To extend the scope of application of this mechanical model, further
11 experimental tests are needed.

12 *4.2.1. Proposed shear strength model for the composite beams with interface* 13 *cracking of the experimental programme*

14 Fig. 10a depicts a simplified representation of the observed shear strength mechanism by
15 means of a strut-and-tie model for the specimen NWP3B2 test, which is an example of a test
16 with more extended interface cracking. Fig. 10a represents the two shear transmission
17 paths that were observed in the composite beams with interface cracking; one through the
18 precast beam and another one through the cast-in-place slab.

19 The shear strength mechanism of the precast beam is explained by means of a strut-and-tie
20 model composed of two superimposed trusses. In this model, the struts represent the
21 compressive stresses carried by the beam's web and the aggregate interlock in the shear
22 cracks. The finite-dimensional nodes at the level of the tension longitudinal reinforcement
23 (see Fig. 10a) represent the dowel action of this reinforcement. The shear strength of the
24 cast-in-place slab is modelled with a simple truss strut-and-tie model without shear
25 reinforcement. Both triangulated bar structures are connected to one another by finite-
26 dimensional nodes at the interface. There are mainly two considered horizontal forces that

1 act at these nodes: the dowel action of transverse reinforcement in the interface crack and
 2 the force resulting from the aggregate interlock in the interface crack (Fig. 10b). The vertical
 3 forces that converge in nodes are considered self-balanced in each part independently
 4 (precast beam on one side and slab on the other) so that the transmission of vertical forces
 5 between the beam and slab is neglected in this model.



7 Fig. 10. Proposed strut-and-tie model of the shear strength mechanism developed by specimen NWP3B2: (a)
 8 precast beam and cast-in-place slab models; (b) forces at the finite-dimensional nodes of the interface crack.

9 In the composite beams of this experimental programme with an extended interface
 10 cracking (NWP1B2, NWP2B2, NWP3B2, HWP6B2, DWP7B2a, DWP7B2b), three different
 11 variants of the strut-and-tie model represented in Fig. 10 were observed which depend on
 12 the extension of the interface crack along the principal span. The calculation procedure of
 13 the shear strength of the specimens with those variants consists on obtaining separately the
 14 component of the total shear at the principal span that is resisted by the precast beam (V_{pb})
 15 and the component of the total shear transmitted by the slab (V_s). Two possible failure
 16 modes were observed at the slab: bending failure ($V_{s,BF}$) or shear failure ($V_{s,SF}$). Thus, the
 17 shear strength of the composite element estimated with the proposed model (V_{pred}) is
 18 calculated as:

$$V_{pred} = V_{pb} + V_s = V_{pb} + \min\{V_{s,BF}, V_{s,SF}\} \quad (1)$$

19 The proposed formulation for the calculation of those shear components is explained in
 20 Annex B.

1 The results of calculating the shear strength of the precast beam and the slab by means of
 2 the proposed calculation methodology are shown in [Table 5](#).

3 *Table 5. Main results of the proposed shear strength model for the composite specimens of the experimental*
 4 *programme with extended interface cracking.*

Specimen	V_{pb} (kN)	$V_{s,BF}$ (kN)	$V_{s,SF}$ (kN)	V_{pred} (kN)	$V_{exp}/$ V_{pred}
NWP1B2	107.4	125.1	62.6	170.0	1.21
NWP2B2	108.2	75.1	70.1	178.3	1.04
NWP3B2	108.2	52.6	72.7	160.8	1.05
HWP6B2	116.6	133.8	69.0	185.6	1.00
DWP7B2a	108.2	52.6	72.4	160.8	1.04
DWP7B2b	108.2	75.1	74.9	183.1	0.98

5 The proposed model for the precast beam provided a similar V_{pb} result for all the studied
 6 specimens ([Table 5](#)). The obtained difference lay in the yield strength of stirrups' steel.

7 In specimens NWP1B2, NWP2B2, HWP6B2 and DWP7B2b, the lowest shear strength
 8 calculated in the slab was obtained from the shear failure criterion ($V_{s,SF}$). Hence according
 9 to the proposed model, these specimens accomplished their shear strength after exceeding
 10 the slab's ultimate shear. On the contrary, specimens NWP3B2 and DWP7B2a had a lower
 11 slab shear strength when it was obtained from the bending failure criterion ($V_{s,BF}$), which
 12 indicated that their shear strength was given by the yielding of the slab's longitudinal
 13 reinforcement prior to the slab's shear failure.

14 Despite adapting the model to the crack pattern of specimen NWP1B2, the model showed a
 15 very safe approximation to the actual value ($V_{exp}/V_{pred} = 1.21$), which could be due to the
 16 anomalous result of this specimen, which presented overstrength compared to the other
 17 specimens with section type B2 (see Section 3.4). Even so, the described model offered a
 18 good approximation to the experimental results, with a mean V_{exp}/V_{pred} value of 1.05 and a
 19 7.06% coefficient of variation for the six analysed specimens.

1 4.2.2. Experimental evidence for the proposed model

2 There are several experimental results that support the adequacy of the proposed model to
3 the shear strength behaviour shown by the composite specimens with extended interface
4 cracking.

5 The stress reached by the stirrups of the principal span at V_{exp} at their mid-length was yield
6 strength, or it came close to it in most cases (see Table 4). In general, stirrup w4 (Fig. 4a)
7 had a lower stress, which could be because it was not crossed by a diagonal crack near the
8 strain gauge location, and also because it was located close to the point load area. However,
9 it is considered acceptable for the model to adopt the simplification of this stirrup also
10 achieving its yield strength because this assumption does not significantly affect the result.

11 Regarding the cast-in-place slab model, the strain gauges located on the concrete surface on
12 top of the slab in Sections A and B (Fig. 4a) of the composite specimens with extended
13 interface cracking measured strains consistently with the tensile or compressive forces
14 considered in the model. In Section B, strain gauges showed compression throughout the
15 test ($\varepsilon_{c,SB}$ in Table 4). However in Section A, gauges measured compression strains in the
16 first test stages, but then changed towards tension strains. At V_{exp} the strains measured in
17 Section A ($\varepsilon_{c,SA}$ in Table 4) were mainly negative (tension). The model represented in Fig.
18 10 illustrates this change from the compression strains near Section B to the tension strains
19 near Section A in the upper slab part.

20 Regarding the cast-in-place slab failure type, in the specimens in which the proposed model
21 indicated shear failure (NWP1B2, NWP2B2, HWP6B2, DWP7B2b), a diagonal crack that
22 crossed the slab in the direction to the point load appeared immediately after V_{exp} (see Fig.
23 8). That diagonal crack did not show any signs of starting from the bending cracks in the
24 slab but originated from within the slab (see the crack located between nodes 4 and 15 of
25 the slab in Fig. B.1b). This justifies using Kupfer failure criterion [39] described herein in
26 Annex B to calculate the shear strength of the slab failing in shear $V_{s,SF}$. In these specimens,

1 the appearance of this diagonal crack took place along with a marked drop in shear, as
2 observed on the shear-deflection relation curves (Fig. 7), typical of brittle shear failures.
3 The specimens in which the proposed model indicated a bending failure of the slab
4 (NWP3B2 and DWP7B2a) showed a very gradual decrease in shear after V_{exp} , typical of
5 ductile failures due to bending.

6 *4.2.3. General application of the proposed model to the composite specimens*

7 As observed in the formulation of the proposed model, the use of one strut-and-tie model
8 or another of the depicted in Fig. B.1, depends on how far the interface crack extends along
9 the principal span. This is difficult to know prior to testing, during the design or in strength
10 assessment phases.

11 The model proposed for specimens NWP3B2 and DWP7B2a (Variant A in Fig. B.1), in which
12 the interface crack length is maximum because it covers the entire principal span, provided
13 the lowest V_{pred} values, which were achieved by the yielding of the slab's longitudinal
14 reinforcement.

15 If the crack length at the interface is not known, adopting the Variant A of the proposed
16 model (see Annex B) to calculate the shear strength of the composite specimens will give a
17 result on the safety side, which will be a lower bound of the shear strength that these
18 specimens can develop. This model is also the simplest of the three proposed variants since
19 the slab's shear strength is given by the yielding of the slab's longitudinal reinforcement, so
20 it does not require doing iterative calculations. Only the formulas of Table B.1 for Variant A
21 and the equation B.1 would be used.

22 Section 5 analyses the extent to which the proposed model was on the safety side for the
23 composite specimens in this experimental programme by assuming that the interface crack
24 length was maximum in them all.

5. Comparison of test results with existing code provisions and the proposed model

5.1. Vertical shear strength

In order to assess the vertical shear strength of the test specimens, the formulations of the following current design codes for the elements with shear reinforcement were used: EC2 [12], MC-10 [13] at its three approximation levels, and the two formulations of ACI 318-19 [10] (named (a) and (b) in Section 22.5.5.1). The composite specimens were also assessed with the proposed model as herein indicated in Section 4.4; that is, considering that the interface crack extended along the entire principal span in all specimens. With all the formulations, the tested average values of the materials were used. The partial safety factors for concrete (γ_c) and steel material properties (γ_s) were 1.0.

Table 6 shows the mean value and the coefficient of variation (CV) of the V_{exp}/V_{pred} ratio for each set of specimens assessed by the different formulations. These statistical indicators were used to analyse the studied sample, bearing in mind that the number of elements in the sample should have been higher for these indicators to take a significant value. To analyse the accuracy of the formulations in predicting shear strength, the 17 experimental programme specimens (excluding HWP6A1 due to test process failure) were grouped into three sets: nine monolithic specimens; six composite specimens with concretes of similar compressive strengths in both the beam and slab (series NW and DW); two composite specimens with different compressive strength concretes in both the beam and slab (series HW). In the composite specimens, shear strength was calculated by different methods considering that: only the precast beam resisted shear, for which the effective beam depth (d_b) and the compressive strength of the beam's concrete ($f_{c,b}$) were used; and the entire composite beam resisted shear, for which the used parameters were the composite beam's effective depth (d_c) and the beam's concrete strength ($f_{c,b}$), the slab's concrete strength ($f_{c,s}$)

1 or the weighted average of the concrete strengths of both the beam and slab estimated from
 2 the area ratio ($f_{c,wa}$). For the composite specimens of series NW and DW, Table 6 shows only
 3 the value calculated with $f_{c,wa}$ because it hardly differed from the values calculated with $f_{c,b}$
 4 or $f_{c,s}$ as these specimens were made by concretes with similar compressive strengths. No
 5 formulation for any specimen offered unsafe results.

6 Table 6. Statistical indicators of the V_{exp}/V_{pred} ratio for the test specimens (specimen HWP6A1 not included: test
 7 process failure).

Specimens	No. of specimens	Method	EC2		MC-10 LI		MC-10 LII		MC-10 LIII		ACI 318-19 (a)		ACI 318-19 (b)		Proposed model	
			Mean	CV (%)	Mean	CV (%)	Mean	CV (%)	Mean	CV (%)	Mean	CV (%)	Mean	CV (%)	Mean	CV (%)
Monolithic	9	$d_b, f_{c,b}$	1.17	8.13	1.68	8.13	1.46	7.85	1.18	6.88	1.41	7.05	1.20	6.93	-	-
Composite (NW, DW)	6	$d_b, f_{c,b}$	1.46	20.23	2.10	20.23	2.02	7.89	1.67	7.22	1.81	18.99	1.47	16.35	-	-
		$d_c, f_{c,wa}$	1.13	7.42	1.63	7.42	1.44	7.91	1.19	7.62	1.40	6.92	1.20	6.88	1.14	7.84
Composite (HW)	2	$d_b, f_{c,b}$	1.57	4.06	2.26	4.06	1.97	4.06	1.55	2.55	1.81	1.55	1.43	1.00	-	-
		$d_c, f_{c,b}$	1.10	4.06	1.59	4.06	1.40	4.06	1.10	2.58	1.27	1.55	1.07	1.14	1.12	3.81
		$d_c, f_{c,s}$	1.10	4.06	1.59	4.06	1.40	4.06	1.19	0.52	1.42	0.86	1.23	1.78	1.12	3.81
		$d_c, f_{c,wa}$	1.10	4.06	1.59	4.06	1.40	4.06	1.12	2.31	1.30	1.11	1.10	0.62	1.12	3.81

8 In the monolithic specimens, EC2 gave the closest approximation to the actual strength, with
 9 adequate scattering (see Table 6). Its formulation was also easy to apply. The LI and LII of
 10 MC-10 offered very safe results. Nonetheless, MC-10 LIII gave a good approximation, which
 11 came close to that of EC2, but its application could prove more difficult given its iterative
 12 formulation. ACI 318-19 (a) gave a safe result, while (b) gave a more accurate value, like
 13 those of EC2 and MC-10 LIII, and was still easy to calculate.

14 In Section 10.9.3(8), EC2 offers the possibility of designing precast elements with a concrete
 15 topping as composite elements, but it does not indicate how. With the results in Table 6, and
 16 as expected, the result obtained when considering only the precast beam (d_b) laid very
 17 much on the safety side in all the composite specimens. However, when the composite beam
 18 depth (d_c) was considered, a result closer to the actual one was obtained with very little
 19 dispersion, and in both the specimens with the same concretes (mean value of 1.13) and
 20 different concretes (1.10). Note that the EC2 formulation did not depend on the
 21 compressive strength of the concrete for the specimens in this experimental programme.

1 As MC-10 does not mention the shear treatment that the composite elements must receive,
2 its shear formulation for assessing monolithic elements' shear strength was used to predict
3 the shear strength of the composite specimens in this experimental programme, and its
4 accuracy was analysed. Firstly, a very safe result was observed if only the precast beam (d_b)
5 was considered. If the entire composite beam's effective depth (d_c) was contemplated, both
6 LI and LII, which do not depend on the concrete compressive strength, still gave very safe
7 results. LIII, which is a function of concrete compressive strength, gave an adequate result
8 for the specimens of series NW and DW (mean value of 1.19), similarly to that obtained for
9 the monolithic specimens (1.18). The most accurate result for the two specimens of series
10 HW, with a higher concrete compressive strength in the beam than in the slab, was obtained
11 when $f_{c,b}$ was used (1.10).

12 ACI 318-19 indicates in Section 22.5.4 that the composite specimens' shear strength can be
13 calculated with the individual elements' properties, which would be comparable to using
14 $f_{c,wa}$ [9,11], or the properties of the element that result in the most critical value; that is,
15 employing the lowest value of $f_{c,b}$ and $f_{c,s}$. Formulation (a) offered results that were very
16 much on the safety side compared to (b), and both were very simple to apply. In the beams
17 of series NW and DW, formulation (b) showed a good result (mean value of 1.20), although
18 it was less precise than that of EC2 (1.13). In the two specimens of series HW, $f_{c,wa}$ gave a
19 very good mean value (1.10) with a very low CV (0.62%), while the use of the lower
20 compressive strength of either the beam or slab, which was that of the slab in this
21 experimental programme, gave a very safe result. As expected, the calculation done with $f_{c,b}$
22 gave a closer result to the actual one (1.07), but its use is not considered in ACI 318-19.

23 Finally, employing the model proposed in Section 4.4 of this paper for the composite
24 elements led to good precision, on the safety side and with low dispersion for both
25 specimens of similar concretes in the beam and the slab (mean value of 1.14) and for
26 different concretes (1.12). The obtained results were very similar to those of EC2 in both
27 cases (1.13 and 1.10, respectively) and to that of ACI 318-19 (b) for series HW (1.10). It

1 should be noted from the proposed model that it is based on a composite beam mechanical
 2 model that is supported by the experimental results, in which the component of the shear
 3 resisted by the precast beam and the component resisted by the slab are calculated by
 4 assuming that interface cracking occurs. Furthermore, the model does not depend on the
 5 concrete compressive strength of both the beam and slab as the shear component resisted
 6 by the beam depends on the yield strength of stirrups' steel, while the shear component
 7 resisted by the slab depends on the yield strength of the steel of the slab's longitudinal
 8 reinforcement.

9 **5.2. Interface shear**

10 **Table 7** offers the mean value and the coefficient of variation (CV) of the relation between
 11 the experimental interface shear stress $\tau_{h,exp}$ concurrent with V_{exp} (see **Table 2**), calculated
 12 as explained in Section 3.2, and the predicted interface shear stress by design codes $\tau_{h,pred}$
 13 for the composite specimens. The formulations of the following design codes for shear at
 14 the interface between the concretes in the elements with reinforcement crossing the
 15 interface were used: EC2 [12], MC-10 [13] and ACI 318-19 [10]. The coefficients indicated
 16 in each code for smooth interfaces (free surface not intentionally roughened, left without
 17 further treatment after vibration) were considered. The materials' tested average values
 18 were employed with all the formulations. Partial safety factors γ_c and γ_s were 1.0. All the
 19 codes used gave safe results for all the specimens.

20 *Table 7. Statistical indicators of the $\tau_{h,exp}/\tau_{h,pred}$ ratio for the eight composite specimens in the experimental*
 21 *programme.*

Code	EC2	MC-10	ACI 318-19
Mean	2.97	4.97	6.11
CV (%)	5.84	5.88	6.67

22 All the codes presented very conservative results for the interface shear of the specimens in
 23 this programme, whose $\tau_{h,exp}$ represented a lower bound of the specimen's interface shear,
 24 calculated for the maximum experimental vertical shear strength V_{exp} as specimens did not
 25 fail in interface shear. The EC2 formulation, based on the Mohr-Coulomb failure criterion,

1 was that which most closely approximated the experimental result, which almost tripled
2 $\tau_{h,pred}$ (see Table 7). The MC-10 formulation, which is very similar to that of EC2, gave a safer
3 result with a similar CV. In both cases, the term of the formula that considers the existence
4 of compressive stress resulting from an eventual normal force acting on the interface,
5 multiplied by a friction coefficient, was neglected, which is usual in designs, given the
6 difficulty to quantify this stress in such elements. If it had been considered, a higher $\tau_{h,pred}$
7 would have been obtained. For ACI 318-19, the formulation limits interface shear to 0.55
8 MPa when the interface is not intentionally roughened, regardless of the existence or
9 nonexistence of reinforcement crossing the interface. Hence a very safe result was obtained.

10 **6. Summary and Conclusions**

11 The objective of this paper was to analyse the shear strength mechanism of composite
12 reinforced concrete beams with web reinforcement. To do so, 18 specimens of rectangular
13 cross-section were experimentally tested, in which the following parameters that influence
14 shear strength varied: the cross-sectional depth, the existence of an interface between
15 concretes, the strengths of both the beam and slab's concretes and differential shrinkage
16 between concretes. A mechanical model was proposed to assess the shear strength of the
17 composite elements in the experimental programme based on the experimental
18 observations. Finally, the formulations to calculate the vertical and interface shear strengths
19 of different current design codes were verified. The main conclusions were as follows:

- 20 1. Placing a cast-in-place slab on top of the precast beam increased the element's shear
21 strength. The shear strength of the composite beam made with concretes of similar
22 compressive strengths in both the precast beam and cast-in-place slab was higher than
23 the shear strength of only the precast beam, and was similar to the shear strength of a
24 monolithic beam with the same depth as the composite beam, made of concrete whose
25 compressive strength was similar to that of the composite beam.

- 1 2. In general, the existence of an interface between concretes modified the crack pattern
2 of the composite beams *versus* that of monolithic beams by forcing diagonal cracks to
3 develop along the interface.
- 4 3. In the composite beams with a similar concrete compressive strength in both the beam
5 and slab, the existence of an interface did not significantly modify the element's shear
6 strength, regardless of the interface presenting more or less cracking, while the
7 composite beams with higher concrete compressive strength in the precast beam than
8 in the slab showed lower shear strengths than their homologous monolithic specimens
9 made with the same concrete as that of the precast beam. Consequently, the shear
10 strength of the composite beams analysed in this experimental programme depended
11 on the concrete compressive strength of the slab or the compression chord.
- 12 4. The major differential shrinkage between the concretes of both the beam and slab did
13 not significantly modify the shear strength of the composite beams in this experimental
14 programme in relation to that of those specimens with reduced differential shrinkage.
- 15 5. The experimental observations indicated that in the composite specimens with
16 extended interface cracking, shear was transmitted through two load paths: one part
17 through the precast beam and the other through the cast-in-place slab. Consequently,
18 the total shear resisted by the composite beam had two components: the shear resisted
19 by the precast beam and the shear resisted by the cast-in-place slab. The transmission
20 of horizontal forces between both load paths occurred through the interface crack due
21 to the aggregate interlock at the crack and the dowel action of the transverse
22 reinforcement crossing the crack.
- 23 6. The mechanical model proposed to assess the shear strength of the composite elements
24 in this experimental programme adapted to each specimen's crack pattern. The shear
25 transmission through the precast beam was modelled using a double truss strut-and-tie
26 model in which the failure criterion was the yielding of stirrups. The shear transmission
27 through the cast-in-place slab was modelled by a simple truss strut-and-tie model

1 without shear reinforcement in which two possible failures were considered: the slab's
2 bending failure due to the yielding of the slab's longitudinal reinforcement or the slab's
3 shear failure when its concrete stresses reached the Kupfer's failure surface. The models
4 adopted for each specimen in the experimental programme offered a very accurate
5 approximation of the actual shear strength with a low coefficient of variation.

6 7. If the interface crack extension is unknown, the mechanical model proposed to calculate
7 shear strength is that formulated for the composite beams showing the greatest
8 interface cracking, in which the slab's failure is due to the yielding of the slab's
9 longitudinal reinforcement, because it predicts a safe result for the element's shear
10 strength. This model does not depend on the concrete compressive strength of both the
11 beam and slab.

12 8. While assessing the shear strength of the composite specimens with the different
13 current design formulations, considering that only the precast beam resists shear gave
14 a very safe result in all cases. When the entire composite beam depth was used, the EC2
15 formulation [12], which does not depend on the concrete compressive strength in the
16 specimens in this experimental programme, gave very good results that were similar to
17 those obtained by applying the model herein proposed; approximation levels I and II of
18 MC-10 [13] provided very safe results, while level III presented a better approximation,
19 especially when the compressive strength of the precast beam's concrete was used to
20 assess the composite beams with different concretes. As for the two formulations of ACI
21 318-19 [10], formulation (a), which is simpler, was very much on the safety side in all
22 cases, while (b) gave very good results when the weighted average of the beam and
23 slab's concrete compressive strengths was used. The formulations for the interface
24 shear offered very safe results with employing the three codes.

25 This research work has increased the number of experimental tests on reinforced concrete
26 composite beams with transverse reinforcement and has contributed to the study of the
27 shear strength mechanism developed by such elements. It should be noted that the above

1 conclusions were drawn for a limited number of specimens and that more tests should be
2 run to reach relevant conclusions. In order to delve into the analysis of the shear strength
3 mechanism and to improve the proposed model, tests should be done on elements with
4 different dimensions and cross-sectional shapes.

5 **Acknowledgements**

6 The experimental programme of this research work was undertaken at the Concrete Science
7 and Technology University Institute (ICITECH) of the Universitat Politècnica de València
8 (UPV; Spain) with concrete supplied by Caplansa. The project was supported by the Spanish
9 Ministry of Science and Innovation through Projects BIA2015-64672-C4-4-R and RTI2018-
10 099091-B-C21-AR; the Regional Government of Valencia through Project AICO/2018/250;
11 the European Union with FEDER funds. The authors thank the Spanish Ministry of Economy
12 and Business for Grant BES-2016-078010 that supported Lisbel Rueda-García.

13 **References**

- 14 [1] Comité technique 4.3 - Ponts routiers Technical Committee 4.3 - Road Bridges.
15 Estimation of load carrying capacity of bridges based on damage and deficiency.
16 PIARC World Road Association: 2016.
- 17 [2] Halicka A. Influence new-to-old concrete interface qualities on the behaviour of
18 support zones of composite concrete beams. *Constr Build Mater* 2011;4072–8.
- 19 [3] Saemann and Washa, G. W. J.C. Horizontal Shear Connections between Precast Beams
20 and Cast-in-Place Slabs. *ACI J Proc* 1964;61:1383–409.
- 21 [4] Loov RE, Patnaik AK. Horizontal Shear Strength of Composite Concrete Beams With
22 a Rough Interface. *PCI J* 1994;39:48–69.
- 23 [5] Kahn LF, Slapkus A. Interface Shear in High Strength Composite T-Beams. *PCI J*
24 2004;49:102–10.

- 1 [6] Kovach J, Naito C. Horizontal Shear Capacity of Composite Concrete Beams without
2 Interface Ties. ATLSS Report No. 05-09: 2008.
- 3 [7] Fang Z, Jiang H, Liu A, Feng J, Chen Y. Horizontal Shear Behaviors of Normal Weight
4 and Lightweight Concrete Composite T-Beams. *Int J Concr Struct Mater* 2018;12.
5 <https://doi.org/10.1186/s40069-018-0274-3>.
- 6 [8] Mahmoud MA, Elafandy TH, Okail HO, Abdelrahman AA. Interfacial shear behavior of
7 composite flanged concrete beams. *HBRC J* 2014;10:206–14.
- 8 [9] Kim C-G, Park H-G, Hong G-H, Kang S-M. Shear strength of composite beams with dual
9 concrete strengths. *ACI Struct J* 2016;113:263–74.
- 10 [10] ACI Committee 318. Building code requirements for structural concrete (ACI 318-
11 19); and commentary (ACI 318R-19). Farmington Hills: American Concrete Institute;
12 2019.
- 13 [11] Kim C-G, Park H-G, Hong G-H, Kang S-M, Lee H. Shear Strength of Concrete Composite
14 Beams with Shear Reinforcements. *ACI Struct J* 2017;114:827–37.
- 15 [12] CEN. EN 1992-1-1:2004. Eurocode 2: Design of concrete structures - Part 1-1:
16 General rules and rules for buildings. 2004.
- 17 [13] Fédération International du Béton (fib). Model Code 2010. Ernst & Sohn; 2012.
- 18 [14] Hernandez G. Strength of Prestressed Concrete Beams with Web Reinforcement.
19 1958.
- 20 [15] Olesen S, Sozen MA, Siess CP. Investigation of prestressed reinforced concrete for
21 highway bridges, part IV, strength in shear of beams with web reinforcement. 1967.
- 22 [16] Hartmann DL, Breen JE, Kreger ME. Shear capacity of high strength prestressed
23 concrete girders. Austin: 1988.
- 24 [17] Shahawy MA, Batchelor B deV. Shear Behavior of Full-Scale Prestressed Concrete

- 1 Girders: Comparison Between AASHTO Specifications and LRFD Code. PCI J
2 1996;41:48–62. <https://doi.org/10.15554/pcij.05011996.48.62>.
- 3 [18] Cumming, A David., Shield, Carol K., French CE. Shear Capacity of High-Strength
4 Concrete Pre-stressed Girders. 1998.
- 5 [19] Runzell B, Shield C, French C. Shear Capacity of Prestressed Concrete Beams. 2007.
- 6 [20] Hawkins NM, Kuchma DA. Application of LRFD Bridge Design Specifications to High-
7 Strength Structural Concrete: Shear Provisions. 2007.
- 8 [21] Avenidaño AR, Bayrak O. Shear strength and behaviour of prestressed concrete
9 beams. Technical Report: IAC-88-5DD1A003-3, Texas Department of
10 Transportation: 2008.
- 11 [22] Hamilton III HR, Llanos G, Ross BE. Shear performance of existing prestressed
12 concrete bridge girders. 2009.
- 13 [23] Ross BE, Ansley MH, Hamilton III HR. Load testing of 30-year-old AASHTO Type III
14 highway bridge girders. PCI J 2011;56.
- 15 [24] Halicka A, Jabłoński Ł. Shear failure mechanism of composite concrete T-shaped
16 beams. Proc Inst Civ Eng Struct Build 2016;169:67–75.
- 17 [25] Jabłoński Ł, Halicka A. Influence of the interface reinforcement on static performance
18 of concrete composite T-shaped beams. Bud i Archit 2020;19:063–76.
19 <https://doi.org/10.35784/bud-arch.2170>.
- 20 [26] Rueda-García L, Bonet Senach JL, Miguel Sosa PF, Fernández Prada MÁ. Experimental
21 analysis of the shear strength of composite concrete beams without web
22 reinforcement. Eng Struct 2021;229:111664.
23 <https://doi.org/10.1016/j.engstruct.2020.111664>.
- 24 [27] Kani MW, Mark W. Huggins, Rudi R. Wittkopp. Kani on shear in reinforced concrete.

- 1 Toronto: University of Toronto, Dept. of Civil Engineering; 1979.
- 2 [28] Rueda-García L, Bonet Senach JL, Miguel Sosa PF. Experimental study of concrete
3 composite beams subjected to shear. Proc. fib Symp. 2019 Concr. - Innov. Mater. Des.
4 Struct., 2019, p. 1779–86.
- 5 [29] UNE-EN 12350-2:2020. Testing fresh concrete - Part 2: Slump test. 2020.
- 6 [30] UNE-EN 12390-3:2020. Testing hardened concrete - Part 3: Compressive strength of
7 test specimens. 2020.
- 8 [31] UNE-EN 12390-6:2010. Testing hardened concrete - Part 6: Tensile splitting strength
9 of test specimens. 2010.
- 10 [32] UNE-EN 12390-13:2014. Testing hardened concrete - Part 13: Determination of
11 secant modulus of elasticity in compression. 2014.
- 12 [33] Comisión Permanente del Hormigón. EHE-2008. Instrucción de Hormigón
13 Estructural. Ministerio de Fomento. Madrid: 2008.
- 14 [34] UNE-EN ISO 6892-1:2017. Metallic materials - Tensile testing - Part 1: Method of test
15 at room temperature. 2017.
- 16 [35] Palaskas MN, Attiogbe EK, Darwin D. Shear strength of lightly reinforced T-beams. J
17 Am Concr Inst 1981;78:447–55.
- 18 [36] Silfwerbrand J. Stresses and strains in composite concrete beams subjected to
19 differential shrinkage. ACI Struct J 1997;94:347–53.
- 20 [37] Fernández Ruiz M, Muttoni A, Sagaseta J. Shear strength of concrete members
21 without transverse reinforcement: A mechanical approach to consistently account
22 for size and strain effects. Eng Struct 2015;99:360–72.
23 <https://doi.org/10.1016/j.engstruct.2015.05.007>.
- 24 [38] Marí A, Cladera A, Bairán J, Oller E, Ribas C. Shear-flexural strength mechanical model

1 for the design and assessment of reinforced concrete beams subjected to point or
2 distributed loads. Front Struct Civ Eng 2014;8. [https://doi.org/10.1007/s11709-](https://doi.org/10.1007/s11709-014-0081-0)
3 014-0081-0.

4 [39] Kupfer HB, Gerstle KH. Behavior of concrete under biaxial stresses. ASCE J Eng Mech
5 Div 1973;99:853–66.

6 **Appendix A. Nomenclature**

7 These Appendixes contain additional information that is not provided in the main body of
8 the paper for the sake of brevity.

9	a	shear span
10	A_{sl}	area of the cross-section of the slab's longitudinal reinforcement
11	A_{sw}	area of the cross-section of the two legs of a stirrup
12	b	width of concrete section
13	c	concrete cover
14	d	effective depth
15	d'	depth of the slab's longitudinal reinforcement
16	d_b	effective depth of the precast beam
17	d_c	effective depth of the entire composite beam
18	E_c	modulus of elasticity of concrete
19	E_s	modulus of elasticity of reinforcement
20	$f_{c,28}$	compressive strength of the concrete measured in cylinders at the age of 28 days
21	$f_{c,b}$	compressive strength of the beam's concrete measured in cylinders
22	$f_{c,s}$	compressive strength of the slab's concrete measured in cylinders

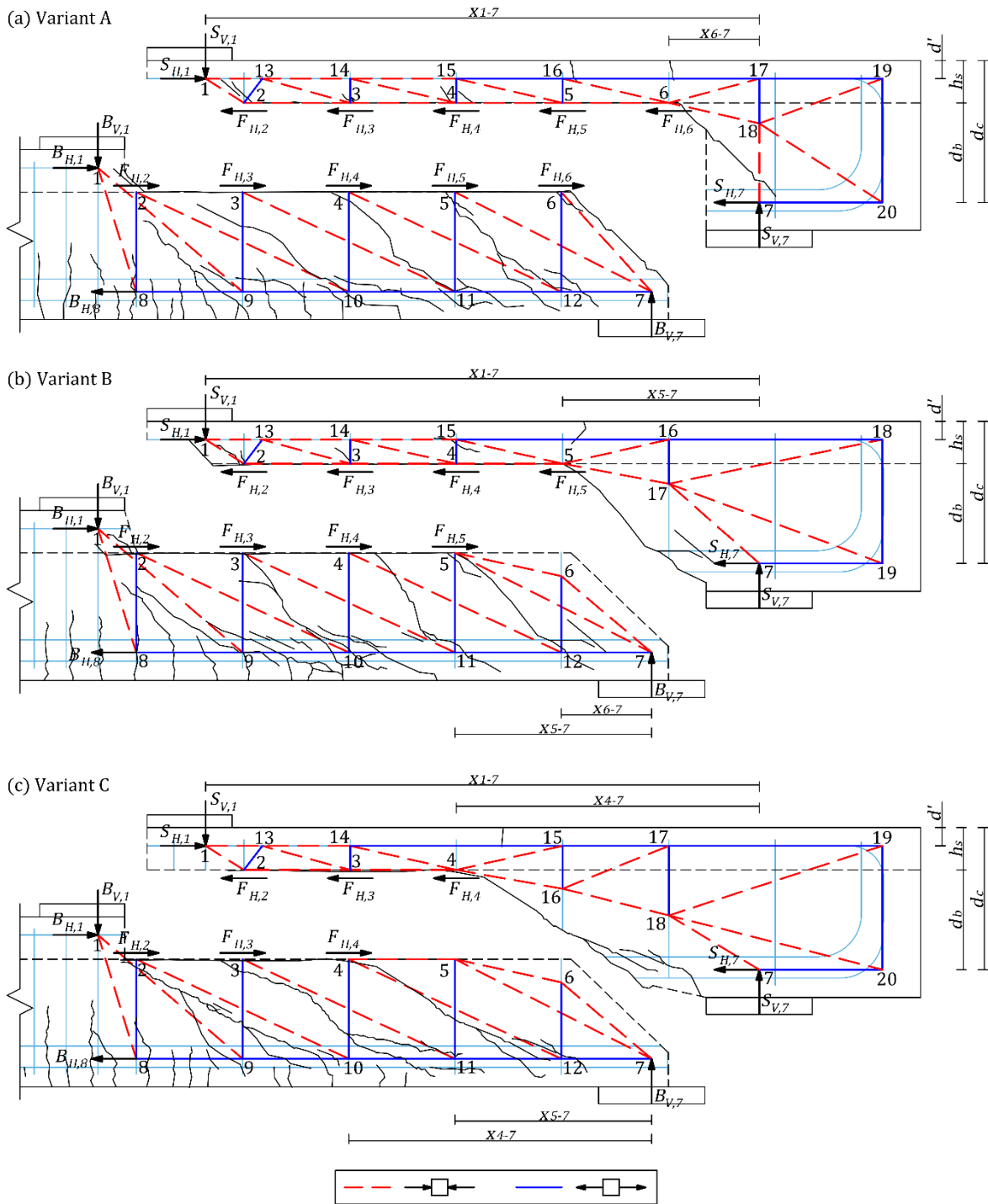
1	$f_{c,wa}$	weighted average of the beam and slab's concrete compressive strengths measured in cylinders estimated from the area ratio
2		
3	f_{ct}	tensile strength of concrete
4	$F_{H,dow}$	experimental horizontal force transferred across the interface crack by web reinforcement
5		
6	$F_{H,exp}$	overall experimental horizontal force at the interface crack of composite specimens
7		
8	$F_{H,int}$	experimental horizontal force transferred across a stretch of the interface crack by means of the aggregate interlock
9		
10	$F_{H,pred}$	overall predicted horizontal force at the interface crack of composite specimens
11	f_u	tensile strength of reinforcement
12	f_y	yield strength of reinforcement
13	h	overall member height
14	h_s	cast-in-place slab height
15	I	moment of inertia of section about the centroidal axis
16	n	number of legs of a stirrup
17	N_s	axial force in the slab
18	\emptyset	nominal diameter of a reinforcing bar
19	T_l	tension force of slab longitudinal reinforcement
20	T_w	tension force of web reinforcement
21	V	shear force
22	$V_{diag,crack}$	shear force corresponding to the first diagonal crack appearing

1	V_{exp}	experimental shear strength
2	V_{pb}	shear strength of the precast beam
3	V_{pred}	predicted value of shear strength
4	V_s	shear strength of the slab
5	$V_{s,BF}$	shear strength of the slab failing in bending
6	$V_{s,SF}$	shear strength of the slab failing in shear
7	γ_c	partial safety factor for concrete material properties
8	γ_s	partial safety factor for steel material properties
9	δ	crack sliding
10	$\varepsilon_{c,Si}$	strain on the concrete surface in section i
11	$\varepsilon_{s,l}$	strain of tension longitudinal reinforcement below the point load
12	ε_u	reinforcement strain at maximum load
13	ε_y	reinforcement strain at yield strength
14	θ	inclination angle of the strut to the horizontal
15	ρ_l	reinforcement ratio of tension longitudinal reinforcement
16	ρ_w	reinforcement ratio of web reinforcement
17	σ_1, σ_2	principal stresses
18	$\sigma_{s,wi}$	stress at the mid-length of stirrup i
19	σ_x	normal stress in the longitudinal direction
20	σ_y	normal stress in the transverse direction
21	τ	tangential stress

- 1 $\tau_{h,exp}$ experimental shear stress at the interface between concretes
- 2 $\tau_{h,pred}$ predicted value of the shear stress at the interface between concretes
- 3 ω crack opening

4 **Appendix B. Formulation of the proposed shear strength model for the**
5 **composite beams with interface cracking of this experimental**
6 **programme**

7 Depending on the extension of the interface crack along the principal span, three different
8 variants of the presented model in Section 4.2 are distinguished. Due to the evident
9 similarity in the crack pattern, Variant A represents the behaviour of the specimens with
10 the more extended interface cracking (NWP3B2 and DWP7B2a), whose strut-and-tie model
11 is represented in [Fig. B.1a](#). Variant B represents the behaviour of the specimens NWP2B2
12 and DWP7B2b ([Fig. B.1b](#)) and Variant C represents the shear strength mechanism of the
13 specimens NWP1B2 and HWP6B2 ([Fig. B.1c](#)).



1

2 Fig. B.1. Proposed strut-and-tie models for the precast beam and the slab separately: (a) Variant
 3 A (specimen NWP3B2); (b) Variant B (specimen NWP2B2); (c) Variant C (specimen NWP1B2).

4 **B.1. Shear strength of the precast beam**

5 Fig. B.1 shows the proposed strut-and-tie models for the precast beam and the slab,
 6 represented as isolated. The shear strength mechanism of the precast beam is explained by
 7 means of a strut-and-tie model composed of two superimposed trusses. Both precast beam
 8 trusses converge at node 7 (see Fig. B.1a). The inclination angle θ of the struts of both

1 trusses is given by the effective depth of the precast beam (d_b in Fig. B.1a) and twice the
2 stirrup spacing, except for the struts of both trusses that converge at the support.

3 Based on experimental observations, the shear that the precast beam can transmit is
4 considered to be limited by the yielding of stirrups' steel. Thus, by using the equilibrium
5 equations and, as the failure criterion, that the tension in stirrups equals $T_w = A_{sw} \cdot f_y$, where
6 A_{sw} is the cross-sectional area of the two legs of a stirrup, V_{pb} is obtained (see Table B.1).
7 The horizontal forces that balance the nodes i in Fig. B.1 (where i is the node identifier)
8 represent the dowel action of the transverse reinforcement at the interface and the
9 aggregate interlock at the interface. Thus, depending on the extension of the interface crack
10 some of these horizontal forces are eliminated. The formulas for calculating these forces for
11 each variant of the model are expressed in Table B.1.

12 *Table B.1. Formulation for the obtaining of the shear strength of the precast beam and the horizontal forces at*
13 *the interface for the three variants of the proposed model.*

Variant	V_{pb}	$F_{H,i}$
A	$V_{pb} = B_{V,7} = 2T_w$	$F_{H,i} = T_w \cdot \cot \theta_i$, where $i = 2, 3, 4, 5, 6$
B		$F_{H,i} = T_w \cdot \cot \theta_i$, where $i = 2, 3, 4$ $F_{H,5} = \frac{T_w(x_{5-7} + x_{6-7})}{d_b}$
C		$F_{H,i} = T_w \cdot \cot \theta_i$, where $i = 2, 3$ $F_{H,4} = \frac{T_w(x_{4-7} + x_{5-7})}{d_b}$

Notation:

x_{j-k} is the horizontal distance between nodes j and k in Fig. B.1.

d_b is the effective depth of the precast beam.

θ_i is the angle formed by the strut that converges at node i with the horizontal.

14 *B.2. Shear strength of the cast-in-place slab*

15 The strut-and-tie model that explains the behaviour of the slab receives the horizontal
16 forces $F_{H,i}$ calculated from the precast beam model, which have equal values and opposite
17 directions (Fig. B.1). The component of the total shear transmitted by the slab (V_s) is
18 represented in the strut-and-tie model by the vertical force at node 7 ($S_{V,7}$). Given the small
19 slab depth and stirrups spacing, stirrups are not considered to contribute to resist shear, so
20 the slab behaves like an element without shear reinforcement. The vertical ties of the truss
21 represent the tension stresses resisted by concrete. The slab is assimilated to a beam with

1 a positive bending moment on the left end (section of node 1 in Fig. B.1a) and a negative
2 bending moment on the right end (section of node 6 in Fig. B.1a).

3 Two possible failure mechanisms in the slab are considered: bending failure of the slab due
4 to yielding of the slab's longitudinal reinforcement or shear failure of the slab. The
5 maximum $S_{V,7}$ that would be transmitted through each mechanism is calculated. The V_s of
6 the model will be the lowest of the shear forces $S_{V,7}$ resisted by each mechanism.

7 *B.2.1. Bending failure of the slab*

8 The model represents the maximum tension force in the slab's longitudinal reinforcement
9 at the slab's right end section. The used failure criterion is, therefore, the force in the
10 horizontal tie (T_l) represented on the end section (ties 16-17, 15-16 and 14-15 in Variant A
11 (Fig. B.1a), Variant B (Fig. B.1b) and Variant C (Fig. B.1c), respectively) is that which
12 corresponds to the yielding of steel ($T_l = A_{sl} f_y$, where A_{sl} is the cross-section area of the
13 slab's longitudinal reinforcement). Using the equilibrium equations in the slab's model and
14 the failure criterion, force $S_{V,7}$ is calculated. When the bending failure of the slab is achieved,
15 force $S_{V,7}$ is identified as $V_{s,BF}$ and is calculated as:

$$V_{s,BF} = \frac{(\sum_{i=2}^K F_{H,i}) \cdot (h_s - d') \cdot d_b + T_l \cdot (h_s - d') \cdot (d_c - d')}{x_{1-7} \cdot d_b - x_{K-7} \cdot (d_c - d')} \quad (\text{B.1})$$

16 where K is the identifier of the node located at the right end of the slab: 6 in Variant A, 5 in
17 Variant B, 4 in Variant C; h_s is the slab's depth (see Fig. B.1); d' is the depth of the slab's
18 longitudinal reinforcement; d_c is the composite beam's effective depth; d_b is the precast
19 beam's effective depth, and x_{j-k} is the horizontal distance between nodes j and k of the slab's
20 model. Forces $F_{H,i}$ are considered positive in the direction indicated in Fig. B.1.

21 *B.2.2. Shear failure of the slab*

22 The slab is considered to be subjected to a biaxial state of stresses. Failure occurs when
23 concrete principal stresses reach the Kupfer's failure surface [39].

1 The principal tensile (σ_1) and compression (σ_2) stresses produced by a set of normal (σ_x
 2 and σ_y) and tangential (τ) stresses are calculated as:

$$\sigma_1 = \frac{\sigma_x + \sigma_y}{2} + \sqrt{\left(\frac{\sigma_x - \sigma_y}{2}\right)^2 + \tau^2} \quad (\text{B.2})$$

$$\sigma_2 = \frac{\sigma_x + \sigma_y}{2} - \sqrt{\left(\frac{\sigma_x - \sigma_y}{2}\right)^2 + \tau^2} \quad (\text{B.3})$$

3 where tensile stress is considered positive.

4 In the specimens of this programme, the normal stresses in the transverse direction to the
 5 slab directrix (σ_y) are considered negligible, and much lower than the normal compressive
 6 stresses parallel to the directrix (σ_x) produced by the axial force on the slab. Shear strength
 7 is calculated on the slab's cross-section with the lowest axial force and highest shear force,
 8 so a section located on the left of the slab's right end (see [Fig. B.1](#)) is taken. The axial force
 9 in slab N_s is obtained as a function of the shear calculated by the slab's shear failure ($V_{s,SF}$)
 10 using the horizontal forces obtained with the precast beam model:

$$N_s = F_{H,K} + \frac{V_{s,SF} \cdot x_{1-7} - (h_s - d') \cdot \sum_{i=2}^K F_{H,i}}{d_c - d'} \quad (\text{B.4})$$

11 where K is the identifier of the node located on the right end of the slab: 6 in Variant A, 5 in
 12 Variant B, 4 in Variant C.

13 With the axial force in the slab, compression stress is calculated as $\sigma_x = -N_s/(b \cdot h_s)$.

14 In Kupfer's failure surface, by assuming the simplification around the corner of the uniaxial
 15 compression envelope as in [38], the relation between the principal stresses is:

$$\sigma_1 = |f_{ct}| + 0.8 \frac{|f_{ct}|}{|f_{c,s}|} \sigma_2 \quad (\text{B.5})$$

16 The tangential stress τ value is obtained by substituting (5) and (6) in (8). By assuming a
 17 parabolic distribution of tangential stresses on the slab's cross-section, the value of the

- 1 shear resisted by the slab in the event of shear failure is obtained as $V_{s,SF} = 2/3 \cdot \tau \cdot b \cdot h_s$. It is
- 2 also verified that $\sigma_1 \leq f_{ct}$ and $\sigma_2 \geq -f_{cs}$. The f_{ct} of the slab's concrete is calculated from
- 3 experimental f_{cs} using the formula provided by EC2 [12].